https://doi.org/10.5194/gmd-2020-415
Preprint. Discussion started: 6 January 2021

Geoscientific Model Development Discussions
Open Access

Simulating $\delta^{15}N$ of atmospheric NO_x in CMAQ version 5.2.1, based on ^{15}N incorporated SMOKE version 4.6 and WRF version 4.0 for assessing the role atmospheric processes plays in controlling the isotopic composition of NO_x, NO_y, and atmospheric nitrate

Huan Fang[†] *and Greg Michalski*[†‡]

[†]Department of Earth, Atmospheric, and Planetary Sciences Purdue University, 550 Stadium Mall Drive, West Lafayette, IN 47907, United States

[‡]Department of Chemistry, Purdue University, 560 Oval Drive, West Lafayette, IN 47907, United States

Correspondence: Huan Fang, fang63@purdue.edu

https://doi.org/10.5194/gmd-2020-415
Preprint. Discussion started: 6 January 2021

Abstract

Nitrogen oxides (NO_x = nitric oxide (NO) + nitrogen dioxides (NO_2)) are important trace gases that affect atmospheric chemistry, air quality, and climate. Despite the importance of NO_x emissions, there are significant uncertainties in NO_x emission inventories. After NO_x from different sources being emitted into the atmosphere, its composition will change due to atmospheric processes. In this study, we used the nitrogen stable isotope composition of NO_x ($\delta^{15}N(NO_x)$) to trace the changes in $\delta^{15}N$ values along the "journey" of atmospheric NO_x, by incorporating ^{15}N into the emission input dataset prepared from the previous companion research (Fang & Michalski, 2020) to run CMAQ (the Community Multiscale Air Quality Modeling System). The simulated spatiotemporal patterns in NO_x isotopic composition were compared with corresponding atmospheric measurements in West Lafayette, Indiana, USA. The results indicate that estimating of atmospheric $\delta^{15}N(NO_x)$ using CMAQ shows better agreement with observation than using SMOKE (Sparse Matrix Operator Kernel Emissions), due to the consideration of mixing, disperse, transport, and deposition of NO_x emission from different sources.

1. Introduction

NO_x (NO_x = NO + NO_2) are important trace gases that affect atmospheric chemistry, air quality, and climate. The NO_x could be converted into NO_y (NO_y = NO_x + HONO + HNO_3 + HNO_4 + N_2O_5 + other N oxides) in the atmospheric NO_x cycle. During this process, the ground-level concentration of O_3 is elevated and secondary particles are generated. Secondary aerosols in turn affect cloud physics, enhancing the reflection of solar radiation (Schwartz, S. E., 1996) and are hazardous to human health (Lighty et al., 2000). Due to its impacts on air quality, climate, human health, and the environment understanding the spatial and temporal variation in the sources of NO_x is a vital scientific question. However, there are still a number of significant uncertainties in the NO_x budget despite years of research. These include a). soil NO_x emissions caused by the application of N fertilizers (Shepherd, 1991; Ludwig et al., 2001; Galloway et al., 2004; Hudman, 2012; Houlton et al., 2013; Pilegaard, 2013) and the role of vegetation (Johansson, 1987; Jacob & Wofsy, 1990; Hanson & Lindberg, 1991; Yienger & Levy II, 1995; Thoene, Rennenberg & Weber, 1996; Slovik et al., 1996; Webber & Rennenberg, 1996; Almaraz et al., 2018); b). emissions from on-road vehicles estimated by different algorithms (Pierson et al., 1996; Singer & Harley, 1996; Cicero-Fernandez et al., 1997; Dreher & Harley, 1998; Dreher & Harley, 1998; Sawyer et al., 2000;

https://doi.org/10.5194/gmd-2020-415
Preprint. Discussion started: 6 January 2021

Parrish, 2006); and c). power plant NO_x emissions due to the implementation of different NO_x emission control technologies (Felix et al., 2012; Srivastava et al., 2005; Xing et al., 2013).

Previous research has shown that there are distinctive differences in $\delta^{15}N$ values for NO_x from different emission sources (Fig. 1), such as soil (Li & Wang, 2008; Felix & Elliott, 2014; Yu & Elliott, 2017; Miller et al., 2018), wastes (Felix & Elliott, 2014), vehicles (Moore, 1977; Heaton, 1990; Ammann et al., 1999; Pearson et al., 2000; Savard et al., 2009; Redling et al., 2013; Fibiger, 2014; Felix & Elliott, 2014; Walters et al., 2015a; Walters et al., 2015b), and power plants (Heaton, 1987; Heaton, 1990; Snape, 2003; Felix et al., 2012; Felix et al., 2015; Walters et al, 2015a; Savard et al., 2017). Thus, the nitrogen stable isotope composition ($\delta^{15}N$) of NO_x could be an effective tracer of atmospheric NO_x sources. The $\delta^{15}N(NO_x)$ is determined by

$$\delta^{15}N(NO_x)\ (‰) = [(^{15}NO_x/^{14}NO_x) / (^{15}N_2/^{14}N_2)_{air} - 1] \times 1000) \qquad \text{Eq. (1)}$$

where $^{15}NO_x/^{14}NO_x$ is the measurement of relative abundance of ^{15}N to ^{14}N in atmospheric NO_x, compared with the ratio of nitrogen in the air, of which has a $^{15}N_2/^{14}N_2 = 0.0036$.

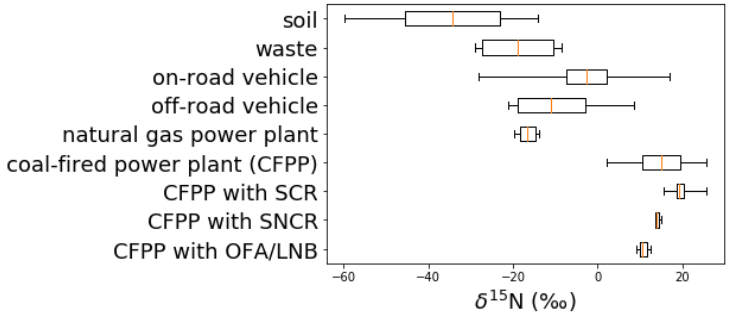

Figure 1: Box (lower quartile, median, upper quartile) and whisker (lower extreme, upper extreme) plot of the distribution of $\delta^{15}N$ values for NO_x emission sources

Here we have simulated the $\delta^{15}N$ values of atmospheric NO_x within the Midwestern United States, under different scenarios, and compared with the recent measurements. The factors required to account for the processes that alter $\delta^{15}N$ of atmospheric NO_x during the NO_x chemical lifetime are: a). The variability of the $\delta^{15}N$ values of NO_x emissions in time and space; b). The transport and mixing of tropospheric NO_x by meteorology; c.) The wet and dry deposition of NO_x/NO_y; and d). The isotope effects occurring during the tropospheric photochemistry that transforms NO_x into NO_y. In a companion paper (Fang & Michalski, 2020), we discussed the effects due to the variation of the $\delta^{15}N$ value of different NO_x emission sources and their variation in time and space. In this

https://doi.org/10.5194/gmd-2020-415
Preprint. Discussion started: 6 January 2021

previous study (Fang & Michalski, 2020), ^{15}N was incorporated into the US EPA trace gas emission model SMOKE (Sparse Matrix Operator Kernel Emissions), in order to simulate the spatiotemporal patterns in the isotopic composition NO_x and compare them with corresponding atmospheric measurements. However, the variability in NO_x emissions over time and space is not sufficient to resolve the spatial and temporal changes in the measured $\delta^{15}N$ values, due to the bias of the static SMOKE output files. For example, NO_x emitted from a single grid cell dominated by a coal-fired power plant would result in a NO_x $\delta^{15}N$ around +12‰. If this grid cell were surrounded by a large array of grid cells dominated by agricultural land-use with a $\delta^{15}N$ of -30‰, the impression is that the region would have a $\delta^{15}N$ value close to -30‰. However, since the power plant emits much more NO_x than the surrounding agricultural fields what would be expected for the actual regional NO_x $\delta^{15}N$ value is biased by the finer emission grid scale. This bias was reduced by weighting each grid cell's NO_x emission relative to the regional total (Fang & Michalski, 2020). In other words, the fine-scale grids were expanded to larger grids, based on assumptions about the NO_x lifetime and transport length scales. This is an unsatisfactory method since the transport of atmospheric NO_x is not controlled by radial diffusion, rather by meteorology/eddy diffusion driven by pressure gradients.

In this work, we explore the effects from the second and third factors, the impacts from atmospheric transport and deposition processes, by incorporating an input dataset of ^{15}N emissions used in simulations by the Chemistry-Transport Model (CTM) used in CMAQ (The Community Multiscale Air Quality Modeling System). We have previously explored the isotope effects arising from tropospheric photochemistry using a 0D box model (Michalski et al., 2020). This ^{15}N isotope reaction scheme will be incorporated into CMAQ as a new chemical mechanism in order to use CMAQ to simulate the $\delta^{15}N$ of NO_y compounds in the subsequent research. The goal of this paper is to explore how atmospheric processes alter the $\delta^{15}N$ of atmospheric NO_x in time and space in the Midwestern US in the absence of isotope effects occurring during the photochemical transformation of NO_x (source and mixing hypothesis).

2. Methodology

In this study, we investigate the role of meteorological transport and removal processes play in the spatiotemporal distribution of NO_x $\delta^{15}N$ values. The ^{15}N emission dataset previously developed (Fang & Michalski, 2020) was used as input for CMAQ to simulate the meteorological transport effects (advection, eddy diffusion, etc). In addition, CMAQ simulated the effect of NO_x

https://doi.org/10.5194/gmd-2020-415
Preprint. Discussion started: 6 January 2021

(nitrate) removal by dry and wet deposition rate is assessed to determine the role of chemistry and deposition might play in the $\delta^{15}N$ of NO_x and atmospheric nitrate. The isotope effects associated with the photochemical transformation of NO_x into HNO_3 and other higher N oxides are ignored, therefore, this paper only focuses on mixing effects and "lifetime chemistry", which blur the grid specific NO_x $\delta^{15}N$ value across the regional scale. The simulations using the same 2002 National Emission Inventory (NEI) but different meteorology conditions (2002 and 2016) were compared, in order to explore how meteorology condition impacts the atmospheric $\delta^{15}N(NO_x)$. Then simulations using the same meteorology condition (2016) but different emission inventories (2002 NEI and 2016 NEI) were compared, in order to explore how emission inventory impacts the atmospheric $\delta^{15}N(NO_x)$. The simulations cover the full domain and nested domain were conducted, in order to explore and eliminate the bias near the domain boundary.

2.1 The domain of the study

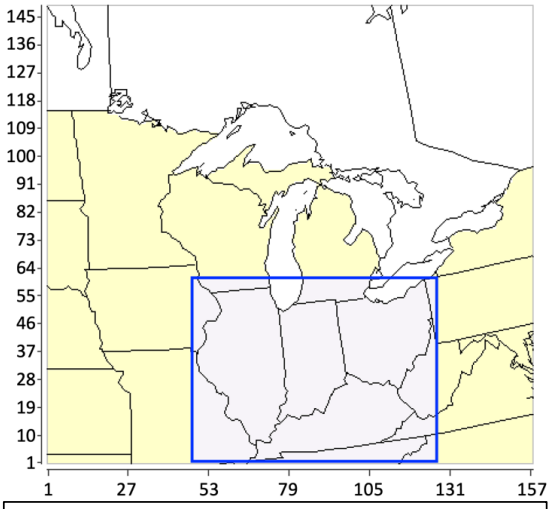

Figure 2: The full geographic domain (yellow) and nested domain (light purple) for the study.

Two domains were used, a larger domain encompassing the Midwestern region of the United States and a smaller nested domain of the central portion of the Midwest domain (Fig. 2). The larger Midwestern domain coordinates ranged from 37 N to 45 N in latitudes, and 98 W to 78 W in longitude. This fully covers the states of Minnesota, Iowa, Missouri, Wisconsin, Illinois, Michigan, Indiana, Kentucky, Ohio, and West Virginia, and partially covers North Dakota, South

https://doi.org/10.5194/gmd-2020-415
Preprint. Discussion started: 6 January 2021

Dakota, Nebraska, Kansas, Tennessee, North Carolina, Virginia, Maryland, Pennsylvania, and New York (Fig. 2, in yellow). A nested domain, which fully covers the states of Indiana, Illinois, Ohio, and Kentucky was extracted (Fig. 2, in light purple), in order to reduce the model bias near the borders that include boundary conditions (details in section 2.6). The horizontal grid resolution for both domains was 12 km x 12 km. The vertical grid resolution is isobaric dependent, which increases with height, from 50 m near the surface (bottom layer) to 600 m near the 50 mb pressure level (top layer).

2.2 $^{15}NO_x$ and $^{14}NO_x$ emission input dataset

The NO_x emission input dataset used by the CTM in CMAQ was prepared, based on the steps described by Fang & Michalski (2020), and are briefly discussed below. The EPA SMOKE model was used to simulate $^{14}NO_x$ emissions. SMOKE converts the annual NO_x emission from county-level emission data contained in the NEI, into hourly emissions and partitions the emission into the gridded format. The emission input datasets were prepared using both the 2002 and 2016 versions of the NEI. The main sources of NO_x emissions in the NEI's are on-road gasoline, on-road diesel, off-road gasoline, off-road diesel, coal-fired power plant, natural gas power plant, soil, and livestock wastes, were categorized into four SMOKE processing categories: Biogenic, Mobile, Point, and Area (Table 1).

The ^{15}N was incorporated into SMOKE outputs, based on NO_x emissions from NEI emission sectors and the corresponding $\delta^{15}N$ values previously discussed (Fang & Michalski, 2020; Table 1). The $^{15}NO_x$ emitted by each SMOKE processing category was calculated based on the definition of $\delta^{15}N$ (‰).

$$^{15}NO_x(i) = {}^{14}NO_x(i) \times {}^{15}R_{NO_x}(i) \qquad \text{Eq. (2)}$$

where $^{14}NO_x$ (i) is the NO_x emissions for each category (i) obtained from NEI and $^{15}R_{NOxi}$ is a ^{15}N emission factor ($^{15}NO_{Xi}/^{14}NO_{xi}$) calculated by:

$$^{15}R_{NO_x}(i) = \left(\frac{\delta^{15}N_{NO_x}(i)}{1000} + 1\right) \times 0.0036 \qquad \text{Eq. (3)}$$

$\delta^{15}N_{NOx(i)}$ is the $\delta^{15}N$ value of each NO_x source category (i = area, biogenic, mobile, and point) (Table 1) and 0.0036 is the $^{15}N/^{14}N$ of air N_2, the reference point for $\delta^{15}N$ measurements. The $\delta^{15}N$ of total NO_x emission was calculated by

$$\delta^{15}N_{NO_x(total)} = \left(\frac{\frac{^{15}NO_x(area)+{}^{15}NO_x(biog)+{}^{15}NO_x(mobile)+{}^{15}NO_x(point)}{^{14}NO_x(area)+{}^{14}NO_x(biog)+{}^{14}NO_x(mobile)+{}^{14}NO_x(point)}}{0.0036} - 1\right) \times 1000 \qquad \text{Eq. (4)}$$

https://doi.org/10.5194/gmd-2020-415
Preprint. Discussion started: 6 January 2021

where

$$^{15}NO_x\ (area) = \left(\frac{\delta^{15}N_{NO_x\ (waste)}}{1000} + 1\right) \times 0.0036 \times {}^{14}NO_x\ (waste)$$

$$+ \left(\frac{\delta^{15}N_{NO_x\ (off-road\ gas)}}{1000} + 1\right) \times 0.0036 \times {}^{14}NO_x\ (off-road\ gas)$$

$$+ \left(\frac{\delta^{15}N_{NO_x\ (off-road\ diesel)}}{1000} + 1\right) \times 0.0036 \times {}^{14}NO_x\ (off-road\ diesel) \qquad \text{Eq. (5)}$$

$$^{15}NO_x\ (mobile) = \left(\frac{\delta^{15}N_{NO_x\ (on-road\ gas)}}{1000} + 1\right) \times 0.0036 \times {}^{14}NO_x\ (on-road\ gas)$$

$$+ \left(\frac{\delta^{15}N_{NO_x\ (on-road\ diesel)}}{1000} + 1\right) \times 0.0036 \times {}^{14}NO_x\ (on-road\ diesel) \qquad \text{Eq. (6)}$$

where $\delta^{15}N_{NO_x\ (on-road\ gas)} = -12.35\ +\ 3.02 \times \ln(t + 0.455)$

Biogenic is NO_x emission from by-products of microbial nitrification and denitrification occurring in the soil; mobile is NO_x emission from the on-road vehicle; the point is NO_x emission from power plants or industry; and the area is all other stationary anthropogenic NO_x emissions, which spread over a spatial extent and individually too small in magnitude to report as point source These include off-road vehicles (utility vehicles for agricultural and residential purposes), residential combustion, industrial processes, agriculture production (livestock waste, fertilizer, etc), etc. Using Eq. (2-6) and $\delta^{15}N$ values from previous research (Table 1), $^{15}NO_x$ emission files were generated from the SMOKE $^{14}NO_x$ output files. The $\delta^{15}N$ of on-road gasoline vehicles was based on the average vehicle travel time (t) within each region with the same zip code (Walters et al., 2015a). The average $\delta^{15}N$ of on-road gasoline vehicles within the study area is -2.7 ± 0.8‰.

SMOKE Category	NEI Sector	$\delta^{15}N$-NO_x (‰) in this study
Biogenic	Soil	-34.3 (Felix & Elliott, 2014)
Area	Livestock Waste	-18.8 (Felix & Elliott, 2014)
	Off-road Gasoline	-11.5 (Walters et al., 2015b)
	Off-road Diesel	-10.5 (Walters et al., 2015b)
Mobile	On-road Gasoline	-2.7 (Walters et al., 2015b)
	On-road Diesel	-2.5 (Walters et al., 2015b)

https://doi.org/10.5194/gmd-2020-415
Preprint. Discussion started: 6 January 2021

Point	Coal-fired EGUs	+15 (Felix et al., 2012)
	Natural Gas EGUs	-16.5 (Walters et al., 2015)

Table 1: $\delta^{15}N$ values for NO_x emission sources by SMOKE processing category and NEI sector

Since the isotope effects associated with the photochemical transformation of NO_x into NO_y are ignored, ^{15}N was not incorporated into the chemical mechanism of CMAQ for the simulations of this research. Therefore, the $^{15}NO_x$ in the emission input dataset acts as a nonreactive chemical. Since $^{14}NO_x$ will go through and be removed in CMAQ's chemical mechanism, the $^{14}NO_x$ in the emission input dataset was replicated and set as a nonreactive chemical. As a result, the mixing effects on the $\delta^{15}N$ of atmospheric NO_x were explored, through the analysis of the time evolution of nonreactive $^{14}NO_x$ and $^{15}NO_x$ concentrations.

2.3 Meteorology input dataset

To explore the impact of atmospheric processes, the meteorology input datasets for the year 2002 and 2016 were prepared and compared. The preparation of the meteorology input datasets for the simulation using CMAQ CTM (CCTM) requires multiple steps. The first step is to generate the input for the CTM meteorological model using the NARR (North American Regional Reanalysis) and NAM (North American Mesoscale Forecast System). Both NARR and NAM Analyses are regional weather model datasets covering North America and were obtained from the National Centers for Environmental Information (2019). NARR and NAM were used to convert the weather observations (every 3 hours for NARR, every 6 hours for NAM Analyses) into gridded meteorological elements, such as temperature, wind field, and precipitation, with the horizontal resolution of 12 km, and 34 vertical layers, with the thickness, increases with height, from 50 m near the surface to 600 m near the 50 mb pressure level. The simulation years were 2002 and 2016 and were selected based on the same timeframe as selected NO_y $\delta^{15}N$ measurements. These include measurements of $\delta^{15}N(NO_3^-)$ at 8 NADP (National Atmospheric Deposition Program) sites within Indiana, Illinois, Ohio, and Kentucky in 2001-03, and the direct measurements of $\delta^{15}N(NO_x)$ between July and August 2016 (Mase, 2010; Riha, 2013).

The second step was to generate the gridded meteorology files on an hourly basis, using the Weather Research and Forecasting Model (WRF) using the input files prepared by the NARR and NAM analyses. To maintain consistency between the NO_x emission dataset and the meteorology, the same coordinate system, spatial domain, and grid size used in the SMOKE model were used

https://doi.org/10.5194/gmd-2020-415
Preprint. Discussion started: 6 January 2021

in the WRF simulation. The same as the emission dataset, the projection type of WRF output is Lambert Conformal, with the standard parallel of 33 N and 45 N, the central meridian of 97 W. The output dataset of WRF has the same spatial domain as the emission dataset with a size of 12 km.

The last step is to prepare the CMAQ-ready meteorology input dataset based on WRF outputs, by running MCIP (the Meteorology-Chemistry Interface Processor), one of the major components of CMAQ. The MCIP first obtains the necessary parameters (Table S1) from WRF outputs. Then the MCIP extracts the data of the necessary parameters for the appropriate geographic domain, which are slightly smaller than the domain of WRF outputs since the cells near the boundary are inadequate for CMAQ simulation. For example, the geographic domain of WRF outputs for this research is 159 grids in the east-west direction and 150 grids in the north-south direction. Therefore, MCIP extracts the WRF outputs into 157 grids in the east-west direction and 148 grins in the north-south direction, which are exactly the same as the emission input dataset prepared from the previous companion research (Fang & Michalski, 2020), and are adequate for CMAQ simulation. After that, MCIP converts the units of the parameters into the units, which are consistent with the CMAQ simulation. For example, the 10-meter wind is displayed as u (east-west) and v (north-south) component of wind vector in WRF but is displayed as wind speed and wind direction in CMAQ. If the parameters, which are necessary for running CMAQ, are not available from the WRF output, MCIP will diagnose and compute them, such as PBL (planetary boundary layer) parameters and cloud information (cloud top, cloud base, liquid water content, cloud coverage). The MCIP also conducts the interpolation and mass-weighted averaging of data, if the grid resolutions of WRF and CMAQ are different. Finally, MCIP organizes the parameters into seven netCDF files that embedded with I/O API (input/output applications programming interface): 2-D time-independent fields at cell centers, 2-D time-independent fields on domain perimeter, 2-D time-independent fields at cell corners, 2-D time-dependent fields at cell centers, 3-D time-dependent fields at cell centers, 3-D time-dependent fields on domain perimeter, and 3-D time-dependent fields at cell corners (Table S2).

2.4 The role of deposition

The dry and wet deposition rates of nonreactive $^{14}NO_x$ and $^{15}NO_x$ were varied to assess their role in the spatiotemporal distribution of NO_x $\delta^{15}N$ value. First, the dry and wet deposition rate of $^{14}NO_x$ and $^{15}NO_x$ was set to zero to test the effect of transport and mixing only. This no-deposition

https://doi.org/10.5194/gmd-2020-415
Preprint. Discussion started: 6 January 2021

simulation was based on 2002 NEI and 2016 meteorology. Next, the dry and wet deposition rate of nonreactive $^{14}NO_x$ and $^{15}NO_x$ was set equal to the CMAQ default (reactive) $^{14}NO_x$ rate in the simulation under the same scenario as the preliminary simulation. An additional simulation under the same scenario, with the amplified dry and wet deposition rate, was conducted, to utilize as the "pseudo tropospheric photochemistry" that removes atmospheric NO_x. To determine the deposition rate of nonreactive $^{14}NO_x$ and $^{15}NO_x$, the initial concentration of NO_x was first magnified to 20 times of the initial concentration derived from the ASCII vertical profiles to represent a relatively polluted atmospheric chemical condition. At the same time, the emission rates of nonreactive $^{14}NO_x$ and $^{15}NO_x$ were set to zero, in order to explore the removal of nonreactive $^{14}NO_x$ and $^{15}NO_x$ by deposition. After the multiple tuning trials, the deposition velocity of nonreactive $^{14}NO_x$ and $^{15}NO_x$ was set to 30 times of the deposition rate of reactive $^{14}NO_x$, of which more than 90% of the nonreactive $^{14}NO_x$ and $^{15}NO_x$ were removed in the simulation period of 2 days. This is in effect the same as simulating the conversion of NO_x into HNO_3, without any isotope effect, without having to alter the chemical mechanism to include ^{15}N. This "pseudo HNO_3" is then removed by wet/dry deposition and the 2-day criteria is the estimated lifetime of NO_x in the atmosphere. By comparing the CMAQ simulation with different settings of NO_x deposition rate, how the removal of atmospheric NO_x by dry and wet deposition impacts the $\delta^{15}N$ of atmospheric NO_x was explored.

2.5 Initial condition and boundary condition for the simulation

The meteorological fields generated by MCIP were used as the inputs for Initial Conditions Processor (ICON) and Boundary Conditions Processor (BCON), used for running CCTM of CMAQ. The ICON program prepares the initial chemical/isotopic concentrations in each of the 3D grid cells for use in the initial time step of the CCTM simulation. For this study, the initial condition was derived from the ASCII vertical profiles to create a "clean" atmospheric chemical condition within the domain at the beginning of the simulation, of which the background concentration of NO_x in each grid is lower than 0.25 ppb. The BCON program prepares the chemical/isotopic boundary condition for throughout the CCTM simulation. Similarly, the boundary condition was derived from the ASCII vertical profiles for this study, which assume a "clean" atmospheric chemical condition (NO_x concentration lower than 0.25 ppb at surface layer) outside the domain.

https://doi.org/10.5194/gmd-2020-415
Preprint. Discussion started: 6 January 2021

The $^{14}NO_x$ in the outputs of ICON and BCON were replicated and set as nonreactive chemical. The same technique was applied to the emission input dataset as well. The nonreactive $^{15}NO_x$ were added to the outputs of ICON and BCON, with the concentration equals to 0.0036 of the concentrations of reactive $^{14}NO_x$, which assumes $\delta^{15}N = 0$ at the initial time step and outside the domain of the simulation (calculated based on Eq. (1-3)). The nonreactive $^{14}NO_x$ and $^{15}NO_x$ do not go through the chemical mechanism within CMAQ so that the effects from tropospheric photochemistry are excluded, thus only atmospheric processes are explored.

2.6 Different versions of the NO_x emission inventory

The simulated $\delta^{15}N$ of atmospheric NO_x based on different emission inventories varies. In order to explore how the difference in $\delta^{15}N$ of NO_x emission impacts the simulated atmospheric NO_x, under the same meteorology conditions, and keep the consistency of the simulation at the same time, two different emission input datasets were prepared. The first dataset was solely based on NEI-2002. The ^{15}N was incorporated into the pre-merged SMOKE output, simulated from each sector of NEI-2002 that contains NO_x emission, based on the corresponding $\delta^{15}N$ values, before merging into the emission input dataset for CCTM simulation. The second dataset, as a comparison, directly obtain the emission rates from the first dataset, except for $^{15}NO_x$. The emission rate of $^{15}NO_x$ was determined by the emission rate of $^{14}NO_x$, obtained from the first dataset, and $\delta^{15}N$ of total NO_x emission, simulated from NO_x emissions from each emission sector based on NEI-2016 and the corresponding $\delta^{15}N$ values determined by the previous companion research (Fang & Michalski, 2020). Thus, the only difference between the two emission input datasets is the $\delta^{15}N$ of the NO_x emission over each grid within the domain.

2.7 The simulation over the nested domain

As mentioned in section 2.5, atmospheric NO_x $\delta^{15}N = 0‰$ for initial condition and boundary condition. As a result, the bias occurs near the border of the research area, mainly under the following two circumstances: a). When the air mass transports out of the research area (Fig. S1) since Canada is considered as "emission-free zone", the atmospheric NO_x is diluted, which impacts its $\delta^{15}N$ values, especially for those with extreme $\delta^{15}N$ values ($\delta^{15}N < -15‰$ or $\delta^{15}N > 5‰$); b). When the air mass with $\delta^{15}N(NO_x)=0$ transports from the "emission-free zone" to the research area (Fig. S2), the atmospheric NO_x is flattened. Therefore, to avoid the bias near the border, the nested domain that only covers Indiana, Illinois, Ohio, and Kentucky was determined, where the

https://doi.org/10.5194/gmd-2020-415
Preprint. Discussion started: 6 January 2021

measurements of $\delta^{15}N$ values at NADP sites are available (Mase, 2010; Riha, 2013). The boundary condition for the simulation over the nested domain is extracted from the CCTM output of the full-domain simulation (BCON code available on Zenodo.org (10.5281/zenodo.4311986)).

https://doi.org/10.5194/gmd-2020-415
Preprint. Discussion started: 6 January 2021

3. Results and Discussion

3.1 Simulated spatial variability in $\delta^{15}N$ of atmospheric NO_x

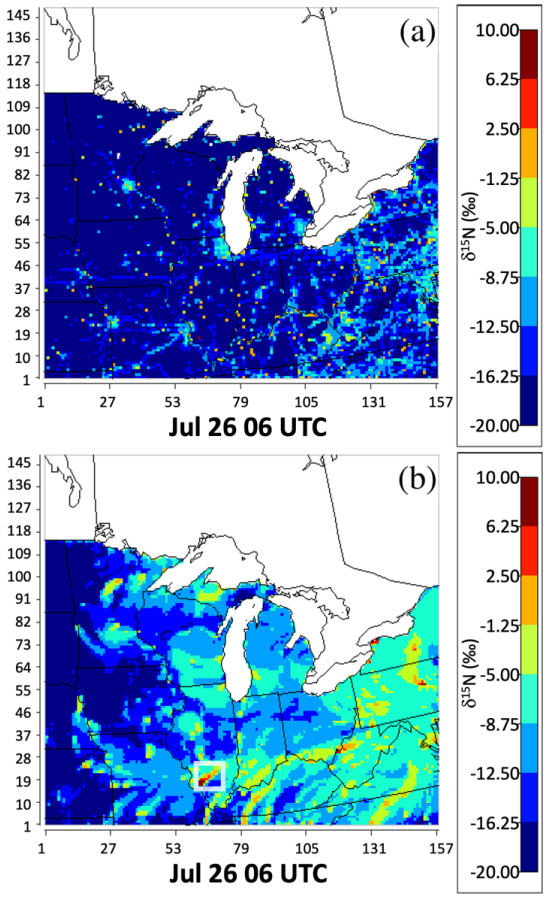

Figure 3: The $\delta^{15}N$ values of NO_x emission, based on NEI-2002 (a: "no transport" scenario) and the $\delta^{15}N$ values of atmospheric NO_x based on NEI-2002 and 2016 meteorology (b: "with transport" scenario), at 06 UTC on July 26, are presented by color in each grid. The warmer the color, the higher $\delta^{15}N$ values of NO_x emission.

https://doi.org/10.5194/gmd-2020-415
Preprint. Discussion started: 6 January 2021

We first examine the spatial heterogeneity of NO_x $\delta^{15}N$ values at a specific time within the Midwestern domain and explore how atmospheric processes alter the $\delta^{15}N$ values relative to the "no transport" simulation. The "no transport" simulation of NO_x $\delta^{15}N$ values (at 06 UTC on July 26) shows that the domain grids ranged from -34.3‰ to 14.9‰ (Figure 3a). The majority of the grids within the domain have NO_x $\delta^{15}N$ values lower than -16.3‰. These low $\delta^{15}N$ values across most of the domain are due to the $\delta^{15}N$ of -34.3‰ for biogenic NO_x emission sources (nitrification and denitrification) in sparsely populated areas where intensive agriculture dominates the land use (Fig. 3a). The $\delta^{15}N$ values of NO_x emitted into grids within big cities mainly ranged between -8.75‰ and -5‰. This is due to the higher fraction of NO_x emission from on-road vehicles having a $\delta^{15}N$ of -2.7 ± 0.8‰. The fraction of NO_x emission from on-road vehicles at the grids resolve major highways is relatively lower, comparing to the grids within big cities, while still higher than most of the grids within the domain. Thus, the $\delta^{15}N$ values along the major highways ranged between -16.25‰ and -8.75‰. The highest value of $\delta^{15}N$ occurs at the grids, where the coal-fired EGUs (+15‰) and hybrid-fired EGUs (using both coal and natural gas (-16.5‰) for combustion) are dominant, showing gold (-1.25‰ ~ +2.5‰) and red/dark red (+2.50‰ and above) on the map (Fig. 3a).

The effect of atmospheric mixing and transport on the NO_x $\delta^{15}N$ spatial distribution were then taken into account by coupling the $^{15}NO_x$ emissions (Fang & Michalski, 2020) to the meteorology simulation. There are significant differences between $\delta^{15}N(NO_x)$ values in the "no transport" (Fig. 3a) and the "with transport" (Fig. 3b) simulations. For example, under the "no transport" scenario (Fig. 3a) the map of $\delta^{15}N(NO_x)$ values clearly shows the locations of big cities, major highways, and power plants, but these features are much less obvious in the "with transport" (Fig. 3b) simulations. The isotopically heavier NO_x emission from big cities, such as Chicago, Detroit, Minneapolis-St Paul, Kansas City, St. Louis, Indianapolis, and Louisville, disperses to the surrounding rural areas so that the $\delta^{15}N(NO_x)$ values in rural areas are elevated to values similar to nearby big cities. Similarly, the NO_x emitted along major highways is transported to the surrounding grids, so that the atmospheric NO_x at the grids around the major highways become isotopically heavier relative to the "no transport" scenario. The most obvious and interesting example is the influence of grids containing coal-fired EGUs on the surrounding region. For example, the EGU located in the southwestern border of the state of Illinois, Baldwin Energy Complex (marked with a transparent white box on Fig. 3b), using refined coal, subbituminous coal, and bituminous coal as its major energy source. The $\delta^{15}N(NO_x)$ in the regions is altered as a

https://doi.org/10.5194/gmd-2020-415
Preprint. Discussion started: 6 January 2021

function of distance away from the EGU and in this time snapshot, the northeastwards propagating plume of NO_x emission from the EGU creates higher $\delta^{15}N(NO_x)$ over 103 km away. Overall, the "with transport" $\delta^{15}N(NO_x)$ map is indicating the emission source that impacts each grid the most, after taking atmospheric mixing and transport into account. The domain average $\delta^{15}N$ increases from -20.23‰ under the "no transport" scenario to -11.49‰ under the "with transport" scenario. The overall emission pattern of the $\delta^{15}N$ value shows that the biogenic emission dominates the spatial domain but after considering the atmospheric processes, anthropogenic emission, mainly from on-road vehicles, becomes dominant over most of the grids, especially for the grids located in the suburb of major cities.

3.2 Seasonal variation in $\delta^{15}N$ of NO_x

https://doi.org/10.5194/gmd-2020-415
Preprint. Discussion started: 6 January 2021

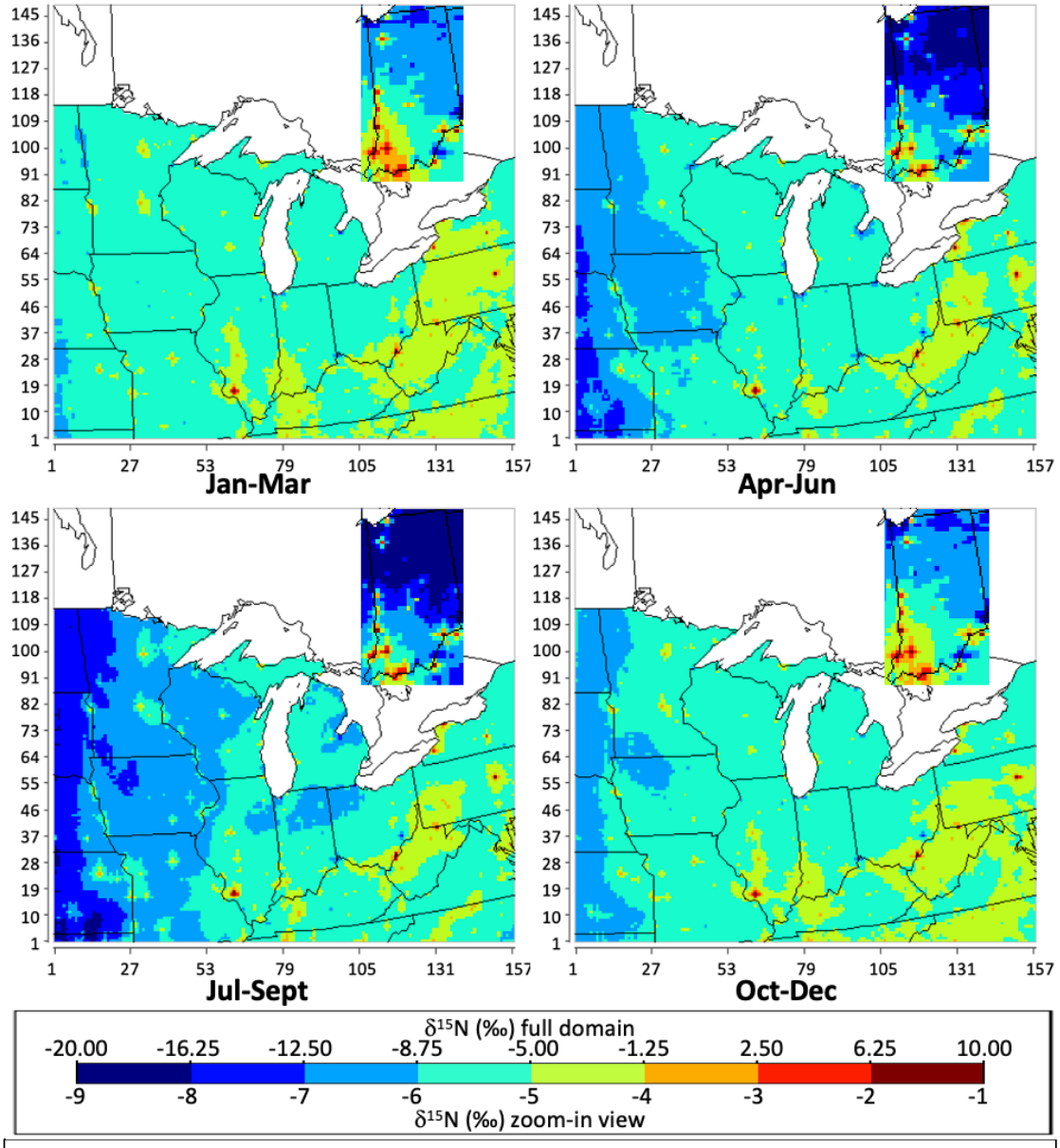

Figure 4: The geographical distribution of the $\delta^{15}N$ value of atmospheric NO_x in each season (Winter: Jan-Mar; Spring: Apr-Jun; Summer: Jul-Sep; Fall: Oct-Dec) in per mil (‰) throughout the Midwest (with zoom-in view focusing on Indiana) simulated by CMAQ, based on NEI-2002 and 2016 meteorology.

We next examine the temporal heterogeneity of atmospheric $\delta^{15}N(NO_x)$ under the "with transport" scenario over the domain and interpret them in terms of changes if the propagation of

https://doi.org/10.5194/gmd-2020-415
Preprint. Discussion started: 6 January 2021

NO_x emission as a function of time. The predicted seasonal average $\delta^{15}N(NO_x)$ in the Midwest shows significant variations (Fig. 4). On an annual basis, the $\delta^{15}N$ values of NO_x range from -19.2‰ to 11.6‰, with the annual average over the Midwest domain of -6.10‰, under the "with transport" scenario. Compared with the seasonal $\delta^{15}N(NO_x)$ under the "no transport" scenario (Fang & Michalski, 2020), the $\delta^{15}N(NO_x)$ under the "with transport" scenario has a similar overall average while narrower range, due to the transport and mixing of the air mass driven by the atmospheric processes. This could be clearly shown on the map, of which the color scheme is smoother, comparing with the seasonal $\delta^{15}N(NO_x)$ under the "no transport" scenario (Fig. S3). The maps for different seasons show the obvious changes in $\delta^{15}N$ values over western regions of the Midwest, from -8.75 ~ -5‰ in Oct-Mar to -16.25 ~ -12.5‰ in Apr-Oct.

In addition to the variability of the NO_x emission source, which has been discussed in depth in the previous companion paper (Fang & Michalski, 2020), the significant temporal variation in the $\delta^{15}N$ value of atmospheric NO_x during different seasons is controlled by the transport and mixing of the air mass, under the different meteorology conditions that vary by season. The PBL height is an effective indicator showing whether the pollutant is under the synoptic condition, which is favorable for the disperse, mixing, and transport after being emitted into the atmosphere (Oke, 2002; Shu et al., 2017; Liao et al., 2018; Miao et al., 2019). In order to qualitatively analyze the changes in $\delta^{15}N$ values driven by atmospheric processes, the difference between the $\delta^{15}N$ value of atmospheric NO_x under the "with transport" scenario and "no transport" scenario ($\Delta\delta^{15}N_{transport}$) on the seasonal basis were shown (Fig. 5). The seasonal $\Delta\delta^{15}N_{transport}$ values range from -21.95‰ to 31.22‰, with an average of 4.93‰. The overall pattern of the $\Delta\delta^{15}N_{transport}$ values shows that after the NO_x being emitted into the atmosphere, it became isotopically heavier over the majority of the grids within the domain, and isotopically lighter over the grids that contain big cities, major highways, and power plants. This could be explained by the transport and disperse of biogenic emission and anthropogenic emission to the surrounding areas. Among the grids located in rural areas, where the biogenic emission dominates the NO_x budget, the $\delta^{15}N$ values increases from around -30‰ to around -10‰, due to transport and disperse of anthropogenic emission with relatively high emission rates from surrounding cities, highways, or power plants, which brings the isotopically heavier NO_x into the grids. On the other hand, among the grids located in the urban area, highways, or power plants, where anthropogenic emission dominates the NO_x budget, the changes in $\delta^{15}N$ values decrease is much less obvious, showing the $\Delta\delta^{15}N_{transport}$ values ranges between -5‰ and +5‰. This could be explained by the relatively high rates of anthropogenic

https://doi.org/10.5194/gmd-2020-415
Preprint. Discussion started: 6 January 2021

emission. Thus, the effects of the transport and disperse of biogenic emissions from the surrounding rural area are minimal.

Comparing the distributions of the difference in $\delta^{15}N$ values (Fig. 5) with the corresponding PBL height (Fig. S4) among the maps of each season, the effects of PBL height on the propagation of the air mass are clearly shown. The PBL height changes significantly among each season within the geographic domain, especially over Minnesota, Wisconsin, and Iowa (Fig. S4). The PBL height over these area increases from less than 250 meters above the ground level to more than 625 meters above the ground level, during spring (Apr-Jun) and summer (Jul-Sep), which creates a more favorable synoptic condition for the disperse, mixing, and transport of the pollutant after being emitted into the atmosphere. As a result, the difference in $\delta^{15}N$ values shifts to higher values, showing the stronger effect of atmospheric processes during spring and summer. The positive correlation between PBL height and propagation of air mass, indicated by the evolution of atmospheric $\delta^{15}N(NO_x)$ in this study, agrees well with the corresponding measurement in megacities in China from the previous studies (Shu et al., 2017; Liu et al., 2018; Liao et al., 2018).

https://doi.org/10.5194/gmd-2020-415
Preprint. Discussion started: 6 January 2021

Geoscientific Model Development Discussions
Open Access

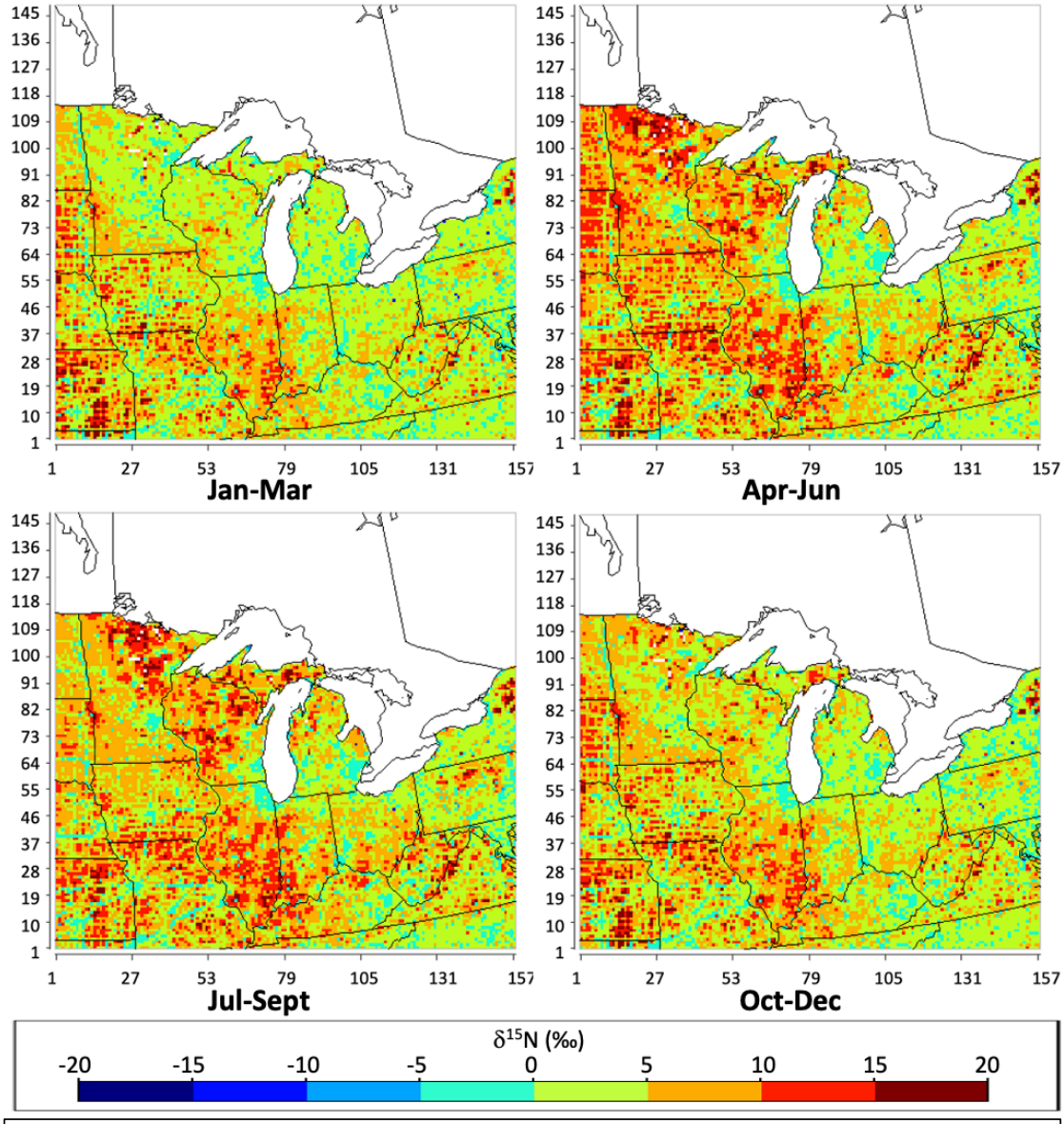

Figure 5: The difference between the $\delta^{15}N$ (‰) value of atmospheric NO_x under the "with transport" scenario and "no transport" scenario ($\Delta\delta^{15}N_{transport}$) during each season (Winter: Jan-Mar; Spring: Apr-Jun; Summer: Jul-Sep; Fall: Oct-Dec), throughout the Midwest simulated by CMAQ, based on NEI-2002 and 2016 meteorology.

https://doi.org/10.5194/gmd-2020-415
Preprint. Discussion started: 6 January 2021

3.3 Different meteorology conditions

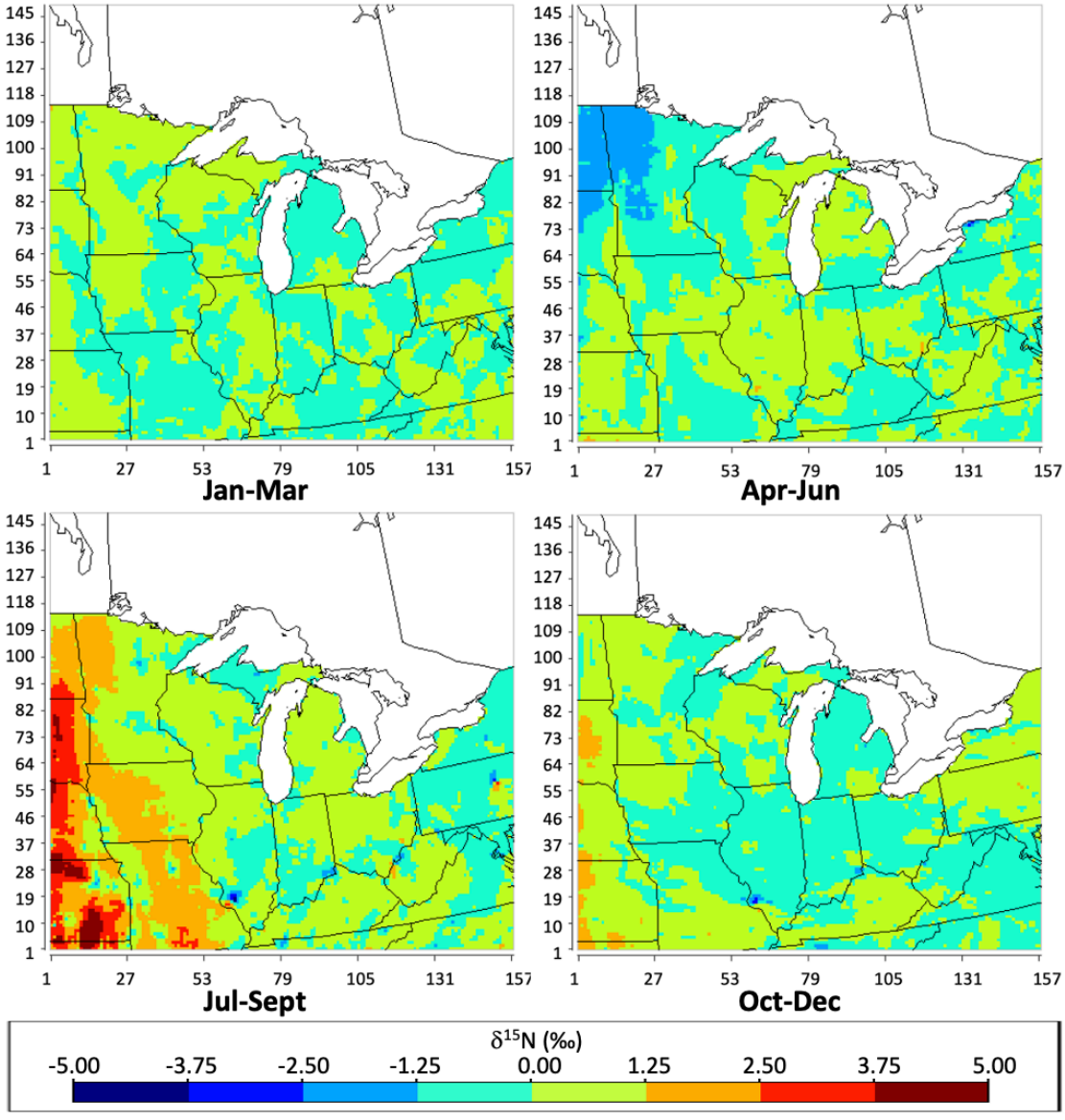

Figure 6: The geographical distribution of the difference between CMAQ simulated $\delta^{15}N$ value of atmospheric NO_x based on 2002 meteorology and 2016 meteorology in each season (Winter: Jan-Mar; Spring: Apr-Jun; Summer: Jul-Sep; Fall: Oct-Dec) in per mil (‰) throughout the Midwest.

https://doi.org/10.5194/gmd-2020-415
Preprint. Discussion started: 6 January 2021

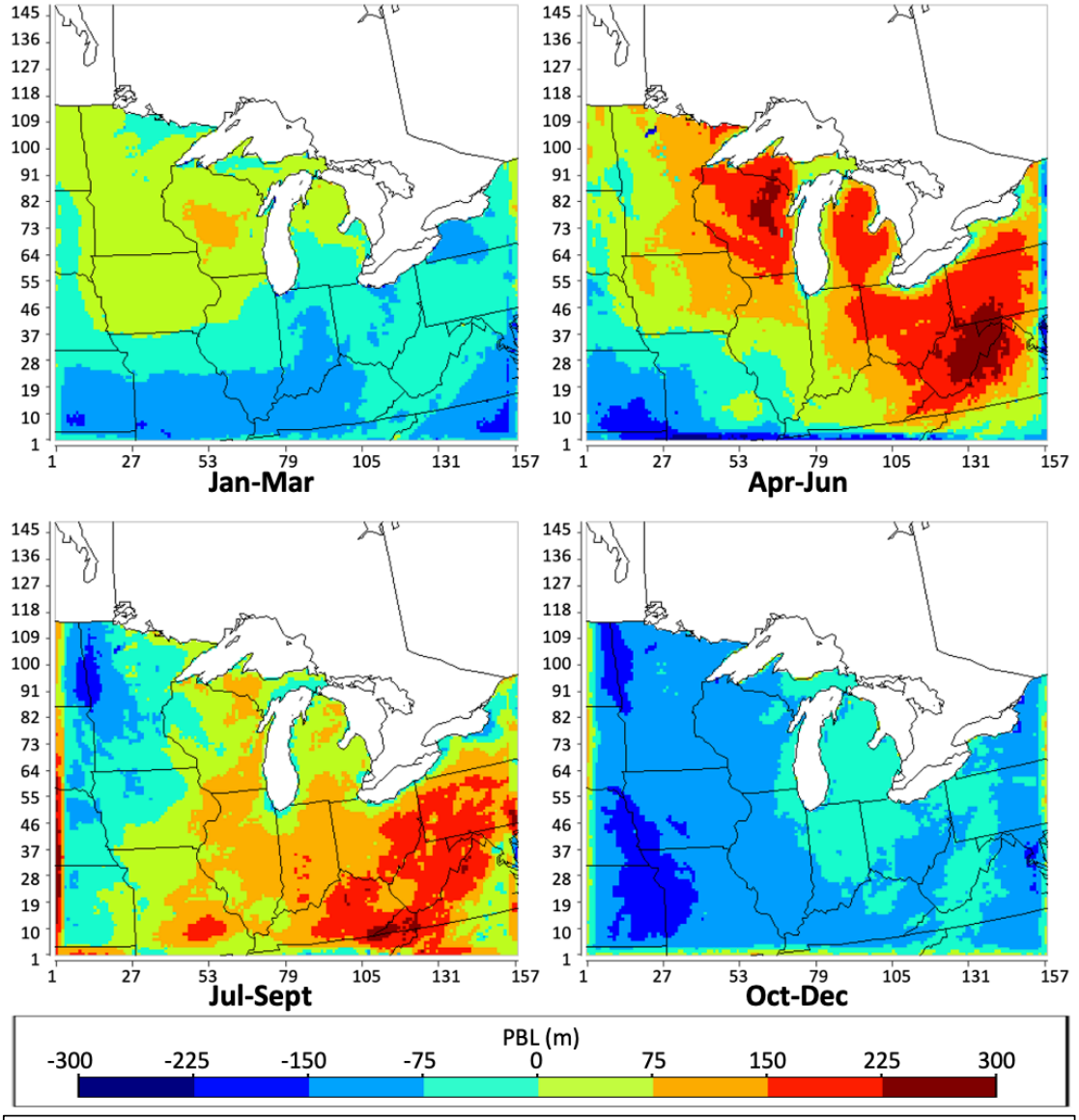

Figure 7: The geographical distribution of the difference between planetary boundary layer (PBL) height in meters based on 2002 meteorology and 2016 meteorology during each season (Winter: Jan-Mar; Spring: Apr-Jun; Summer: Jul-Sep; Fall: Oct-Dec) of 2016 throughout the Midwest.

The atmospheric $\delta^{15}N(NO_x)$ simulated based on different meteorology input dataset varies. In order to compare the spatial heterogeneity of the atmospheric $\delta^{15}N(NO_x)$ under different meteorology conditions, the same analysis was done on the simulation using 2002 meteorology

https://doi.org/10.5194/gmd-2020-415
Preprint. Discussion started: 6 January 2021

(Fig. S6). Overall, the simulated atmospheric NO_x under 2002 meteorology is isotopically heavier than under 2016 meteorology, especially in the western part of the domain during summer (Fig. 6). The dynamics of PBL height potentially cause the variation in the level of disperse, mixing, and transport of NO_x emission. Due to the significantly higher level of PBL during spring and summer (Fig. 7) comparing to the seasonal PBL height during 2016, the disperse, mixing, and transport of anthropogenic NO_x emission with higher $\delta^{15}N$ values alters the atmospheric $\delta^{15}N(NO_x)$ over the rural area further, under 2002 meteorology. The videos of atmospheric $\delta^{15}N(NO_x)$ on an hourly basis throughout the year 2002 and 2016 are available on Zenodo.org (10.5281/zenodo.4311986).

3.4 Different versions of emission inventories

There was a dramatic difference in the atmospheric $\delta^{15}N(NO_x)$ simulated depending on which NEI emission dataset was used. In order to compare the spatial heterogeneity of the atmospheric $\delta^{15}N(NO_x)$ generating from different NO_x emission budgets, the same analysis was done on the simulation using the emission input dataset prepared from the 2016 version of NEI (Fig. S7). In general, the simulated atmospheric NO_x based on 2016 NEI is significantly isotopically lighter than based on 2002 NEI, especially in the central and eastern parts of the domain (Fig. 8). According to Fang & Michalski (2020), the fraction of NO_x emission from the anthropogenic source in NEI-2016 was lower than in NEI-2002 for most of the grids within the domain. Therefore, the atmospheric $\delta^{15}N(NO_x)$ based on 2016 NEI was lower. According to US Energy Information Administration (2017b), from 2002 to 2016, 53 Giga Watts coal-fired and 54 Giga Watts natural gas EGU retired in the US. The EGU dominates the NO_x emission at the grids where it is located in, account for up to 90% of the total NO_x emission (Fang & Michalski, 2020). Given the $\delta^{15}N$ value of the NO_x emitted from coal-fired EGU is +15‰ (Table 1), the $\delta^{15}N$ values of the atmospheric NO_x over the grids that contain the abandoned coal-fired EGU change dramatically during the period between 2002 and 2016. A similar pattern occurs at the grids that contain the EGU, which uses both coal and natural gas as its energy source ($\delta^{15}N$ = -0.75‰). As a result, the number of "hotspots" with high $\delta^{15}N$ values in 2016 is much less than in 2002. While, the change in $\delta^{15}N$ values of the atmospheric NO_x over the grids that contain the abandoned natural gas EGU is not that obvious under the scenario of "with transport" from 2002 to 2016, since the $\delta^{15}N$ value of the NO_x emitted from natural gas EGU is -16.5‰ (Table 1), which is similar to the $\delta^{15}N$ values at the surrounding grids after the mixture of NO_x emission from biogenic source and on-road

https://doi.org/10.5194/gmd-2020-415
Preprint. Discussion started: 6 January 2021

vehicles. Besides this, the implementation of NO_x emission control technologies (SCR, SCNR, LNB, OFA) decreases the $\delta^{15}N$ of the NO_x emission from power plants and vehicles, thus decrease the atmospheric $\delta^{15}N(NO_x)$.

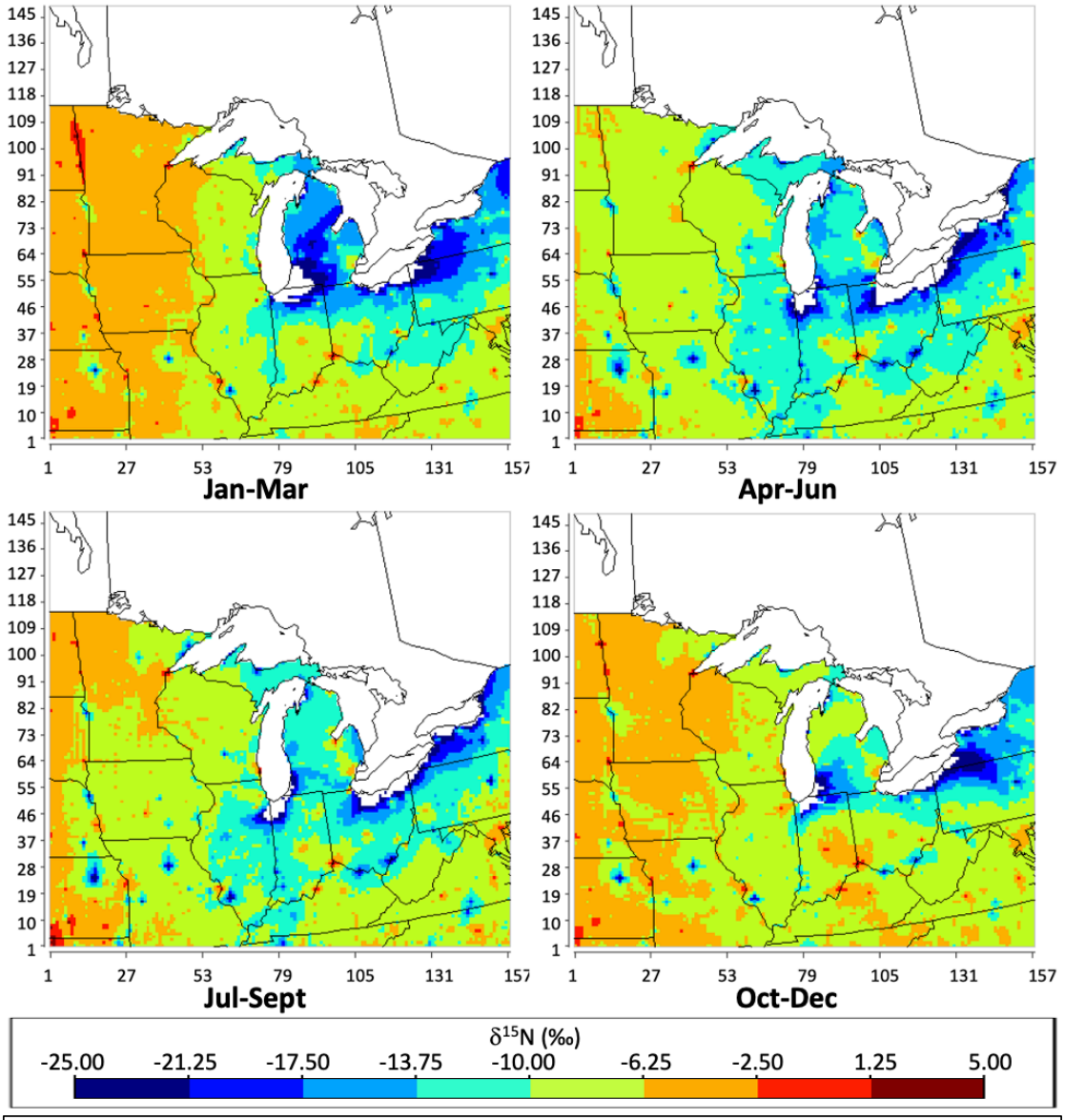

Figure 8: The geographical distribution of the difference between CMAQ simulated $\delta^{15}N$ value of atmospheric NO_x based on NEI-2016 and NEI-2002 in each season (Winter: Jan-Mar; Spring: Apr-Jun; Summer: Jul-Sep; Fall: Oct-Dec) in per mil (‰) throughout the Midwest.

https://doi.org/10.5194/gmd-2020-415
Preprint. Discussion started: 6 January 2021

3.5 The role of deposition

The deposition alters the $\delta^{15}N$ of atmospheric NO_x. In order to compare the spatial heterogeneity of the atmospheric $\delta^{15}N(NO_x)$ with different settings of NO_x deposition rate, the same analysis was done on the simulation using the amplified dry and wet deposition rates (Fig. S8). In order to explore the impact of dry and wet deposition on the $\delta^{15}N$ of atmospheric NO_x, the difference between the $\delta^{15}N$ values of atmospheric NO_x under the "amplified deposition" scenario and "default deposition" scenario ($\Delta\delta^{15}N_{deposition}$) on the seasonal basis were shown (Fig. 9). The seasonal $\Delta\delta^{15}N_{deposition}$ values range from -3.67‰ to 5.34‰, with an average of 0.51‰. The overall pattern of the $\Delta\delta^{15}N_{deposition}$ values shows that due to the impact of deposition, the atmospheric NO_x became isotopically lighter over the majority of the grids within the domain, and isotopically heavier over the grids, which contain or surround power plants and big cities. The amplified deposition simulation somehow presents the isotope effects associated with the "pseudo photochemical transformation" of NO_x into NO_y. The complete isotope effect of tropospheric photochemistry will be addressed in future work, which incorporates ^{15}N into the chemical mechanism of CMAQ for the simulation.

https://doi.org/10.5194/gmd-2020-415
Preprint. Discussion started: 6 January 2021

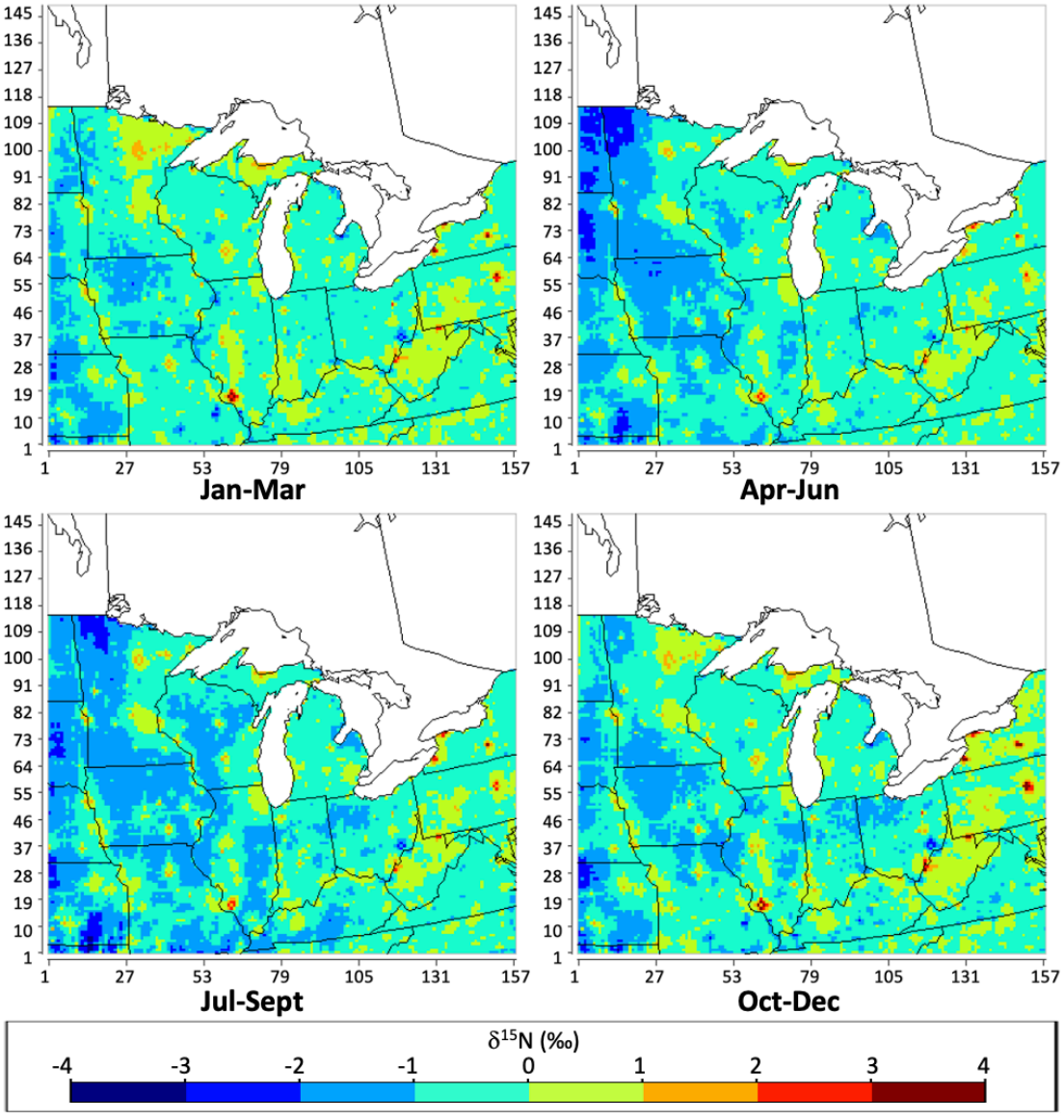

Figure 9: The difference between the $\delta^{15}N$ (‰) value of atmospheric NO_x under the "amplified deposition" scenario and "default deposition" scenario ($\Delta\delta^{15}N_{deposition}$) during each season (Winter: Jan-Mar; Spring: Apr-Jun; Summer: Jul-Sep; Fall: Oct-Dec), throughout the Midwest simulated by CMAQ, based on NEI-2002 and 2016 meteorology.

3.6 The simulation over the nested domain

https://doi.org/10.5194/gmd-2020-415
Preprint. Discussion started: 6 January 2021

We next examine the temporal heterogeneity of difference in atmospheric $\delta^{15}N(NO_x)$ between nested-domain simulation and full-domain simulation ($\Delta\delta^{15}N_{nested\text{-}full}$), to explore the potential bias due to the motion of the air mass across the boundary of the geographic domain of the study (Fig. 10). The nested domain covers the states of Indiana, Illinois, Ohio, and Kentucky, where the measurements of $\delta^{15}N$ values at NADP sites are available. The predicted $\delta^{15}N$ of atmospheric NO_x over the nested domain shows a similar overall pattern as the $\delta^{15}N$ within the same domain from the full-domain simulation, except over the southern border of the domain (Fig. S9). In order to qualitatively analyze the effects from the initial boundary condition, the $\delta^{15}N$ of atmospheric NO_x within IN, IL, OH, and KY were extracted from the full-domain simulation (Fig. 4) and compare with the nested-domain simulation within the same region (Fig. 10). The $\Delta\delta^{15}N_{nested\text{-}full}$ values ranged between -0.25‰ and +0.25‰ over most of the grids within the nested domain, showing the difference between nested-domain simulation and full-domain simulation of $\delta^{15}N$ values are trivial. However, near the southern border of the nested domain, the obvious $\Delta\delta^{15}N_{nested\text{-}full}$ values closed to +0.75‰ during fall and winter, closed to +1.00‰ during spring and summer occur, which indicate the atmospheric NO_x from the nested-domain simulation is isotopically heavier. The values of $\Delta\delta^{15}N_{nested\text{-}full}$ become obvious near the southern border, which indicates the dilution of NO_x, after it transports out of the domain since the $\delta^{15}N$ on the boundary was set to zero. Unlike the southern border, the northern, western, and eastern border of the nested domain is located sufficient distance apart from the boundary of the full domain. As a result, the $\Delta\delta^{15}N_{nested\text{-}full}$ values are similar over the majority grids within the domain.

https://doi.org/10.5194/gmd-2020-415
Preprint. Discussion started: 6 January 2021

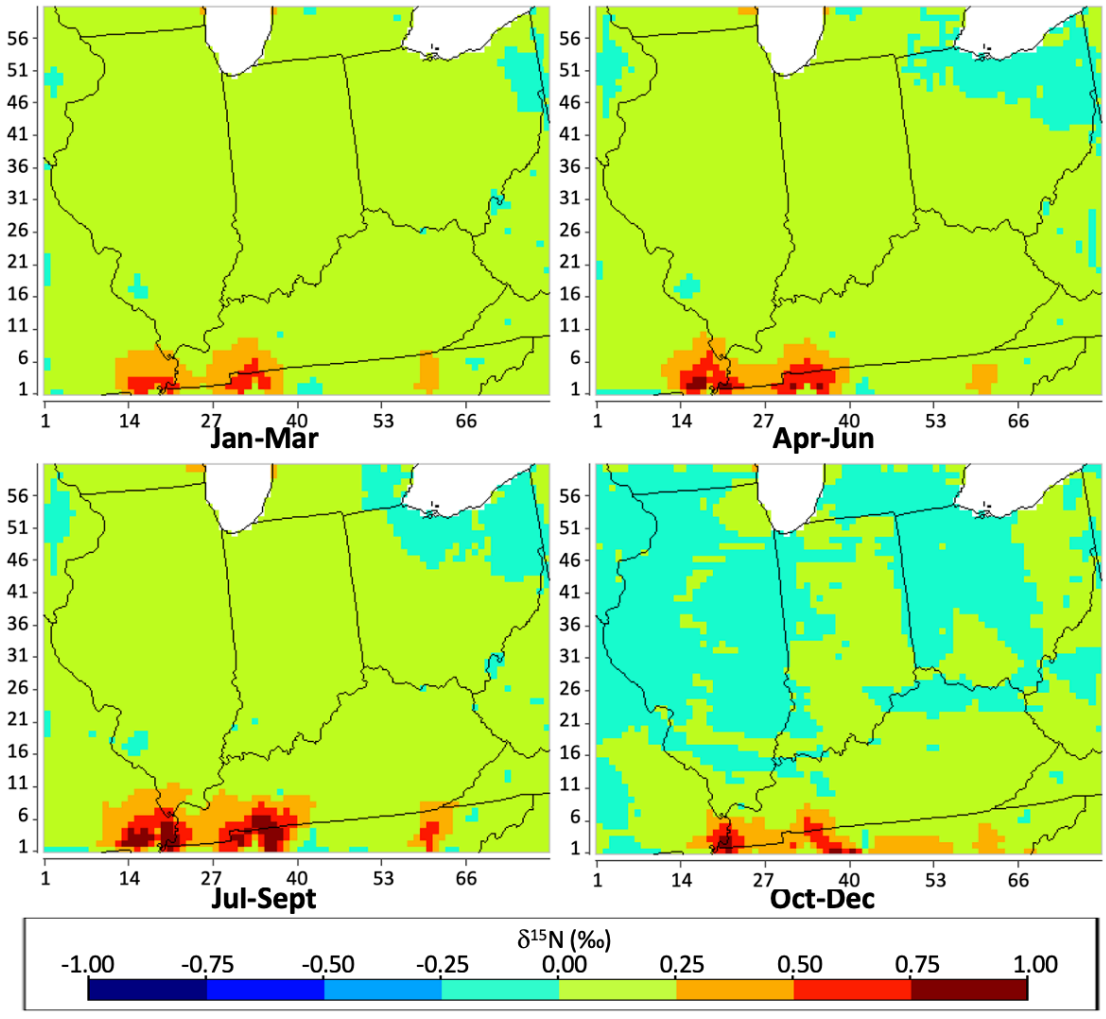

Figure 10: The geographical distribution of the difference between nested-domain simulation and full-domain simulation of $\delta^{15}N$ value of atmospheric NO_x ($\Delta\delta^{15}N_{nested\text{-}full}$) in each season (Winter: Jan-Mar; Spring: Apr-Jun; Summer: Jul-Sep; Fall: Oct-Dec) in per mil (‰) within IN, IL, OH, and KY, based on NEI-2002 and 2016 meteorology.

3.7 Model-observation comparison

https://doi.org/10.5194/gmd-2020-415
Preprint. Discussion started: 6 January 2021

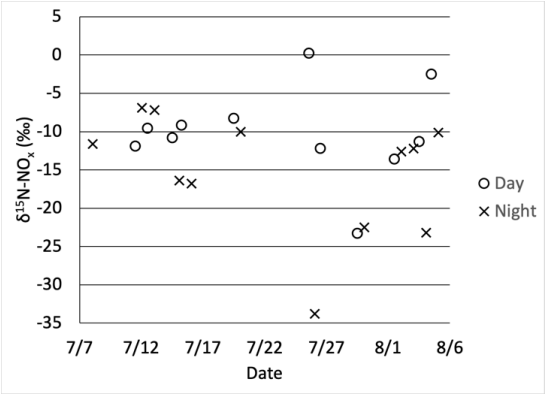

Figure 11: The $\delta^{15}N(NO_x)$ values measured at West Lafayette, IN between July 9 and August 5, 2016, from 8 am to 4 pm during the daytime (○), and from 9:30 pm to 5:30 am during the nighttime (×)

In order to evaluate the CMAQ simulation of atmospheric $\delta^{15}N(NO_x)$, several existing datasets of measurements were utilized to compare with the simulations. As the only direct measurements of $\delta^{15}N(NO_x)$ within the domain, NO_x samples collected between July 8 and August 5, 2016 (Fig. 11; Walters, Fang, & Michalski, 2018) was first used for the validation of the CMAQ simulation. 30 NO_x samples were collected from 8 am to 4 pm during the daytime, and from 9:30 pm to 5:30 am during the nighttime in West Lafayette, IN, an NADP (National Atmospheric Deposition Program) site in the northwest part of Indiana and home to Purdue University. The measured $\delta^{15}N(NO_x)$ ranged from -23.3 to 0.2‰ for the daytime samples and -33.8 to -6.9‰ for the nighttime samples.

https://doi.org/10.5194/gmd-2020-415
Preprint. Discussion started: 6 January 2021

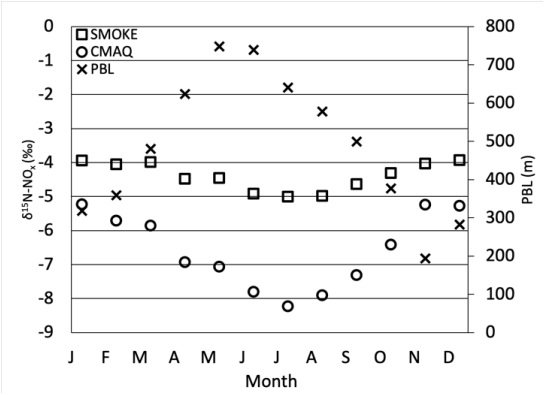

Figure 12: The monthly $\delta^{15}N$ values of total NO_x emission simulated by SMOKE (□) based on NEI-2002, the monthly $\delta^{15}N$ values of atmospheric NO_x simulated by CMAQ (○) based on NEI-2002 and 2016 meteorology, the monthly average of PBL height (×, right axis) over the 12-km grid that covers West Lafayette, IN.

The CMAQ simulated $\delta^{15}N$ values of atmospheric NO_x in West Lafayette show more obvious monthly variations and seasonal trends comparing to the $\delta^{15}N$ values of NO_x emission (Fig. 12, in circle (○)). The simulation shows that the $\delta^{15}N$ of atmospheric NO_x starts around -5‰ in January, which is about 1‰ lower than $\delta^{15}N$ of NO_x emission (Fig. 12, in square (□)). During winter (Jan-Mar), the $\delta^{15}N$ of atmospheric NO_x decrease slightly, and the difference between the $\delta^{15}N$ of NO_x emission gradually increases. During spring (Apr-June), the more obvious decreasing trend of the $\delta^{15}N$ of atmospheric NO_x occurs, and the difference between the $\delta^{15}N$ of NO_x emission is larger than during winter. The $\delta^{15}N$ value reaches the minimum around -8‰ in July. During summer (Jul-Sept), the $\delta^{15}N$ of atmospheric NO_x starts to increase, and the difference between the $\delta^{15}N$ of NO_x emission decreases. During fall (Oct-Dec), the $\delta^{15}N$ of atmospheric NO_x increases, and the difference between the $\delta^{15}N$ of NO_x emission decreases, but with a slighter trend than during summer. The $\delta^{15}N$ of atmospheric NO_x ends at -5‰, 1‰ lower than $\delta^{15}N$ of NO_x emission. In addition to the change in the fractions of NO_x emission sources from April to September, which has been discussed in the previous companion paper (Fang & Michalski, 2020), the monthly variations and seasonal trend of the simulated atmospheric $\delta^{15}N(NO_x)$ are mainly driven by the

https://doi.org/10.5194/gmd-2020-415
Preprint. Discussion started: 6 January 2021

strength of disperse, mixing, and transport of the atmospheric NO_x emitted from different sources, indicated by the PBL height. The PBL height during the period from April to September is 90% higher than during the period from October to March, which is favorable for the mixture of isotopically lighter NO_x from the surrounding area (Fig. 12, in cross (×)). Thus, the $\delta^{15}N$ of atmospheric NO_x diverges further from the $\delta^{15}N$ of NO_x emission.

	measurement	NEI 2002	NEI 2016	NEI-2002 +WRF2016	NEI-2002 +WRF2002	NEI-2016 +WRF2016	NEI-2002 +WRF2016 nested
min	-33.800	-12.180	-18.439	-15.824	-14.779	-31.149	-15.858
max	0.200	-3.753	-4.410	-3.360	-3.726	5.458	-3.187
median	-11.250	-4.993	-7.049	-8.094	-8.355	-13.975	-8.108
stdev	8.023	2.168	2.388	2.081	1.881	4.122	2.099

Table 2: Performance of $\delta^{15}N(NO_x)$ simulation for West Lafayette, IN

The CMAQ simulation of the $\delta^{15}N$ of atmospheric NO_x under different scenarios of NEI and WRF was compared with the measurement (Walters, Fang, & Michalski, 2018) from July 8 to August 5, 2016 (Fig. 13). The $\delta^{15}N$ of atmospheric NO_x simulated based on NEI-2002 and 2016 meteorology ranges from -15.8‰ to -3.4‰, with the medium of -8.1 ± 2.1‰; the $\delta^{15}N$ of atmospheric NO_x simulated based on NEI-2002 and 2002 meteorology ranges from -14.8‰ to -3.7‰, with the medium of -8.4 ± 1.9‰; the $\delta^{15}N$ of atmospheric NO_x simulated based on NEI-2016 and 2016 meteorology ranges from -31.1‰ to -5.5‰, with the medium of -14.0 ± 4.1‰. The $\delta^{15}N$ of the corresponding measurement ranges from -33.8‰ to 0.2‰, with the medium of -11.2 ± 8.0‰. In general, the CMAQ simulations of $\delta^{15}N(NO_x)$ under most of the scenarios conducted in this study, except the simulation based on NEI-2016 and 2016 meteorology, perform better than the SMOKE simulation of $\delta^{15}N(NO_x)$, which only take the variability of NO_x emission source into account (Table 2). On the other hand, the simulation based on NEI-2016 and 2016 meteorology capture the isotopically light NO_x better than the simulations under the other scenarios of emission and meteorology input datasets.

https://doi.org/10.5194/gmd-2020-415
Preprint. Discussion started: 6 January 2021

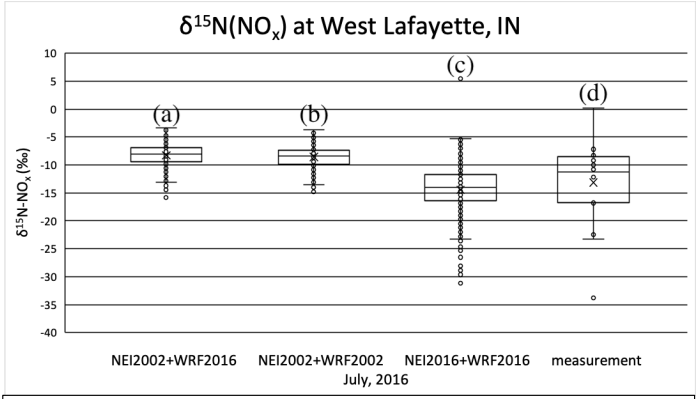

Figure 13: The distributions of $\delta^{15}N(NO_x)$ values over the 12-km grid that covers West Lafayette, IN from July 8 to August 5, simulated by CMAQ, based on NEI-2002 and 2016 meteorology (a), NEI-2002 and 2002 meteorology (b), NEI-2016 and 2016 meteorology (c), compare with the corresponding measurement (d) taken on July to August in 2016 (box: lower quartile, median, upper quartile; whisker: lower extreme, upper extreme; dots outside the whisker: outliers)

Finally, we compared the CMAQ predicted $\delta^{15}N(NO_x)$, under the scenario of NEI-2002+WRF2002 at NADP sites within Indiana, Illinois, Ohio, and Kentucky (Table S3) with the measurements of $\delta^{15}N(NO_3^-)$ from 2001 to 2003. The $\delta^{15}N$ values of atmospheric NO_x simulated by CMAQ at these sites show obvious monthly variations and seasonal trends (Fig. 14, top). The monthly boxes are the 1st and 3rd quantiles of the simulated monthly $\delta^{15}N$ of atmospheric NO_x at the NADP sites. The whiskers represent the minimum and maximum values without outliers. There is a wide range of $\delta^{15}N(NO_x)$ values within each month, with a minimum during January (-7.8~ -4.1‰) and a maximum during August (-11.4~-4.4‰). The seasonal trend shows low $\delta^{15}N(NO_x)$ during summer, with the median around -7.4‰, and high $\delta^{15}N(NO_x)$ during winter, with the median around -6.0‰.

https://doi.org/10.5194/gmd-2020-415
Preprint. Discussion started: 6 January 2021

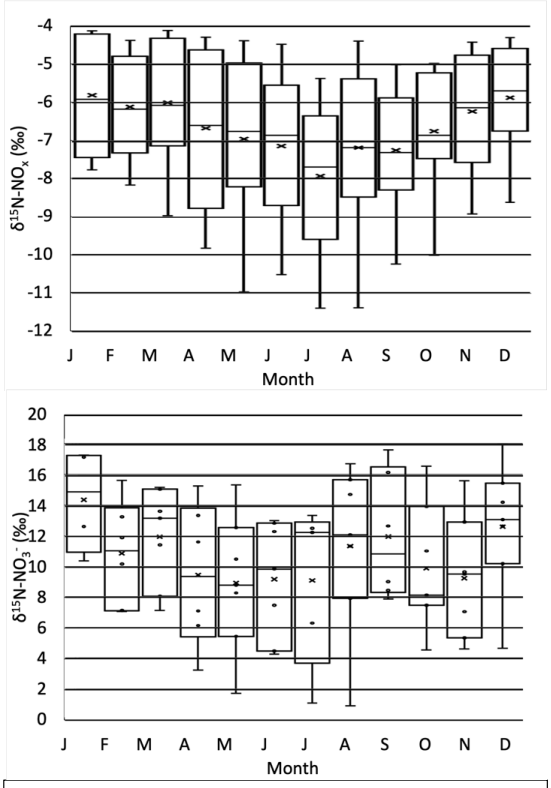

Figure 14: The CMAQ predicted $\delta^{15}N$ value of atmospheric NO_x at NADP sites within IN, IL, OH, and KY (top) using NEI-2002 and 2002 meteorology compared to the measured $\delta^{15}N$ of rain NO_3^- (bottom) from prior studies.

Comparing with the CMAQ simulation, the measurements of $\delta^{15}N$ values of NO_3^- at NADP sites from prior studies (Mase, 2010; Riha, 2013) shows the similar monthly variations and seasonal trend (Fig. 14, bottom). There is a wide range of $\delta^{15}N(NO_3^-)$ values within each month, with a minimum during January (10.4~17.2‰) and a maximum during August (1.0~16.7‰). The seasonal trend shows low $\delta^{15}N(NO_3^-)$ during spring, with the median around 9.3‰, and high $\delta^{15}N(NO_3^-)$ during winter, with the median around 13.0‰. The measured $\delta^{15}N$ values of NO_3^- has the same seasonal trend as the CMAQ simulated $\delta^{15}N$ values of NO_x. However, the measured $\delta^{15}N$ values of NO_3^- is about 17‰ higher than the CMAQ simulated $\delta^{15}N$ values of NO_x. The difference between CMAQ simulated $\delta^{15}N$ values of NO_x and measured $\delta^{15}N$ values of NO_3^- is caused by the

https://doi.org/10.5194/gmd-2020-415
Preprint. Discussion started: 6 January 2021

following two factors: a). the mixture of isotopically lighter NO_x from the surrounding area discussed in section 3.2, and b). the net N isotope effect during the conversion of NO_x to NO_3^-, which will be addressed in future work.

4. Conclusion

The $\delta^{15}N$ of atmospheric NO_x was simulated by CMAQ, based on the emission input datasets prepared from the previous companion research (Fang & Michalski, 2020) and the meteorology input dataset simulated from WRF and MCIP. $\delta^{15}N$ is an effective tool to track the atmospheric NO_x, in term of its evolution of spatial and temporal composition, altered by atmospheric processes. The simulation indicates that the PBL height is the key driver for the mixture of anthropogenic and natural NO_x emission, which deepens the gap between $\delta^{15}N$ of atmospheric NO_x and NO_x emission. Comparing with the measurements of $\delta^{15}N(NO_3^-)$ from NADP sites within Indiana, Illinois, Ohio, and Kentucky, the simulated $\delta^{15}N$ agreed well with the seasonal trend and monthly variation. The performance of CMAQ simulated $\delta^{15}N(NO_x)$ is better than SMOKE $\delta^{15}N(NO_x)$ from the previous companion research (Fang & Michalski, 2020), due to the consideration of mixing, disperse, and transport of NO_x emission from different sources.

After considering the effects of NO_x emission sources and atmospheric processes, there is still an obvious gap between the simulated $\delta^{15}N(NO_x)$ and the corresponding measurements. Therefore, before adjusting the NO_x emission inventory, the future work is to explore how tropospheric photochemistry alters $\delta^{15}N(NO_x)$ by incorporating ^{15}N into the chemical mechanism of CMAQ and comparing the simulation with the corresponding measurements. With the validation of our nitrogen isotopes incorporated CMAQ, the NO_x emission inventories could be effectively evaluated and improved.

Data availability: The in-detail simulation results for $\delta^{15}N$ of atmospheric NO_x under all scenarios discussed in this paper and the CMAQ-based c-shell script for generating BCON for nested domain simulation are achieved on Zenodo.org (10.5281/zenodo.4311986). The source code for CMAQ version 5.2.1 is available at https://github.com/USEPA/CMAQ/tree/5.2.1. The in-detail simulation results for $\delta^{15}N$ of NO_x emission based on 2002 and 2016 versions of National Emission Inventory and the associated python codes are achieved on Zenodo.org (10.5281/zenodo.4048992). The input datasets for WRF simulation are available at https://www.ncei.noaa.gov/data/.

https://doi.org/10.5194/gmd-2020-415
Preprint. Discussion started: 6 January 2021

Author contributions: Huan Fang and Greg Michalski were the investigator for the project and organized the tasks. Huan Fang develops the model codes, reconstruct CMAQ by incorporating ^{15}N and performed the simulation to generated $\delta^{15}N$ values. Greg Michalski helped Huan Fang in interpreting the results. Huan Fang prepared the manuscript with contributions from all co-authors.

Acknowledgments: We would like to thank the Purdue Research Foundation and the Purdue Climate Change Research Center for providing funding for the project. We would like to thank Tomas Ratkus from Department of Earth, Atmospheric, and Planetary Sciences, Steven Plite, and Frank Bakhit from Rosen Center for Advanced Computing, Purdue University for setting up CMAQ on Purdue research computing for this project.

https://doi.org/10.5194/gmd-2020-415
Preprint. Discussion started: 6 January 2021

References:

Almaraz, M., Bai, E., Wang, C., Trousdell, J., Conley, S., Faloona, I. and Houlton, B. Z.: Agriculture is a major source of NOx pollution in California, Sci. Adv., doi:10.1126/sciadv.aao3477, 2018.

Ammann, M., Siegwolf, R., Pichlmayer, F., Suter, M., Saurer, M. and Brunold, C.: Estimating the uptake of traffic-derived NO2 from 15N abundance in Norway spruce needles, Oecologia, doi:10.1007/s004420050710, 1999.

Beirle, S., Spichtinger, N., Stohl, A., Cummins, K. L., Turner, T., Boccippio, D., Cooper, O. R., Wenig, M., Grzegorski, M., Platt, U. and Wagner, T.: Estimating the NOx produced by lightning from GOME and NLDN data: A case study in the Gulf of Mexico, Atmos. Chem. Phys., doi:10.5194/acp-6-1075-2006, 2006.

Boersma, K. F., Eskes, H. J., Meijer, E. W. and Kelder, H. M.: Estimates of lightning NOx production from GOME satellite observations, Atmos. Chem. Phys., doi:10.5194/acp-5-2311-2005, 2005.

Bradshaw, J., Davis, D., Grodzinsky, G., Smyth, S., Newell, R., Sandholm, S. and Liu, S.: Observed distributions of nitrogen oxides in the remote free troposphere from the NASA Global Tropospheric Experiment programs, Rev. Geophys., doi:10.1029/1999RG900015, 2000.

Byun, D., Pleim, J., Tang, R. and Bourgeois, A.: Meteorology-Chemistry Interface Processor (MCIP) for Models-3 Community Multiscale Air Quality (CMAQ) Modeling System, System, 1999.

Chameides, W. L., Davis, D. D., Bradshaw, J., Rodgers, M., Sandholm, S. and Bai, D. B.: An estimate of the NO x production rate in electrified clouds based on NO observations from the GTE/CITE 1 fall 1983 field operation , J. Geophys. Res., doi:10.1029/jd092id02p02153, 1987.

Christian, H. J., Blakeslee, R. J., Boccippio, D. J., Boeck, W. L., Buechler, D. E., Driscoll, K. T., Goodman, S. J., Hall, J. M., Koshak, W. J., Mach, D. M. and Stewart, M. F.: Global frequency

https://doi.org/10.5194/gmd-2020-415
Preprint. Discussion started: 6 January 2021

and distribution of lightning as observed from space by the Optical Transient Detector, J. Geophys. Res. Atmos., doi:10.1029/2002jd002347, 2003.

Cicero-Fernândez, P., Long, J. R. and Winer, A. M.: Effects of Grades and Other Loads on On-Road Emissions of Hydrocarbons and Carbon Monoxide, J. Air Waste Manag. Assoc., doi:10.1080/10473289.1997.10464455, 1997.

Davidson, E. A.: Pulses of nitric oxide and nitrous oxide flux following wetting of dry soil: an assessment of probable sources and importance relative to annual fluxes, Trace gas Exch. a Glob. Perspect., 1992.

Davidson, E. A. and Kingerlee, W.: A global inventory of nitric oxide emissions from soils, Nutr. Cycl. Agroecosystems, doi:10.1023/a:1009738715891, 1997.

De Laeter, J. R., Böhlke, J. K., De Bièvre, P., Hidaka, H., Peiser, H. S., Rosman, K. J. R. and Taylor, P. D. P.: Atomic weights of the elements: Review 2000 (IUPAC Technical Report), Pure Appl. Chem., doi:10.1351/pac200375060683, 2003.

DeCaria, A. J., Pickering, K. E., Stenchikov, G. L. and Ott, L. E.: Lightning-generated NOx and its impact on tropospheric ozone production: A three-dimensional modeling study of a Stratosphere-Troposphere Experiment: Radiation, Aerosols and Ozone (STERAO-A) thunderstorm, J. Geophys. Res. D Atmos., doi:10.1029/2004JD005556, 2005.

Dentener, F. J. and Crutzen, P. J.: Reaction of N2O5 on tropospheric aerosols: impact on the global distributions of NOx, O3, and OH, J. Geophys. Res., doi:10.1029/92JD02979, 1993.

Dreher, D. B. and Harley, R. A.: A fuel-based inventory for heavy-duty diesel truck emissions, J. Air Waste Manag. Assoc., doi:10.1080/10473289.1998.10463686, 1998.

Elliott, E. M., Kendall, C., Boyer, E. W., Burns, D. A., Lear, G. G., Golden, H. E., Harlin, K., Bytnerowicz, A., Butler, T. J. and Glatz, R.: Dual nitrate isotopes in dry deposition: Utility for

https://doi.org/10.5194/gmd-2020-415
Preprint. Discussion started: 6 January 2021

partitioning NO x source contributions to landscape nitrogen deposition, J. Geophys. Res. Biogeosciences, doi:10.1029/2008JG000889, 2009.

Elliott, E. M., Kendall, C., Wankel, S. D., Burns, D. A., Boyer, E. W., Harlin, K., Bain, D. J. and Butler, T. J.: Nitrogen isotopes as indicators of NOx source contributions to atmospheric nitrate deposition across the midwestern and northeastern United States, Environ. Sci. Technol., doi:10.1021/es070898t, 2007.

Fang, H. & Michalski, G.: Incorporating 15N into the outputs of SMOKE version 4.6 as the emission input dataset for CMAQ version 5.2.1 for assessing the role emission sources plays in controlling the isotopic composition of NOx, NOy, and atmospheric nitrate. Geoscientific Model Development, 2020 (submitted).

Fehr, T., Höller, H. and Huntreiser, H.: Model study on production and transport of lightning-produced NOx in a EULINOX supercell storm, J. Geophys. Res. D Atmos., doi:10.1029/2003JD003935, 2004.

Felix, J. D., Elliott, E. M. and Shaw, S. L.: Nitrogen isotopic composition of coal-fired power plant NOx: Influence of emission controls and implications for global emission inventories, Environ. Sci. Technol., doi:10.1021/es203355v, 2012.

Felix, J. D. and Elliott, E. M.: The agricultural history of human-nitrogen interactions as recorded in ice core δ15N-NO3-, Geophys. Res. Lett., doi:10.1002/grl.50209, 2013.

Felix, J. D. and Elliott, E. M.: Isotopic composition of passively collected nitrogen dioxide emissions: Vehicle, soil and livestock source signatures, Atmos. Environ., doi:10.1016/j.atmosenv.2014.04.005, 2014.

Felix, J. D., Elliott, E. M., Avery, G. B., Kieber, R. J., Mead, R. N., Willey, J. D. and Mullaugh, K. M.: Isotopic composition of nitrate in sequential Hurricane Irene precipitation samples: Implications for changing NOx sources, Atmos. Environ., doi:10.1016/j.atmosenv.2015.01.075, 2015.

https://doi.org/10.5194/gmd-2020-415
Preprint. Discussion started: 6 January 2021

Fibiger, D. L., Hastings, M. G., Lew, A. F. and Peltier, R. E.: Collection of NO and NO2 for isotopic analysis of NOx emissions, Anal. Chem., doi:10.1021/ac502968e, 2014.

Fraser, A., Goutail, F., McLinden, C. A., Melo, S. M. L. and Strong, K.: Lightning-produced NO2 observed by two ground-based UV-visible spectrometers at Vanscoy, Saskatchewan in August 2004, Atmos. Chem. Phys., doi:10.5194/acp-7-1683-2007, 2007.

Fujita, E. M., Croes, B. E., Bennett, C. L., Lawson, D. R., Lurmann, F. W. and Main, H. H.: Comparison of emission inventory and ambient concentration ratios of CO, NMOG, and NOx in California's South Coast Air Basin, J. Air Waste Manag. Assoc., doi:10.1080/10473289.1992.10466989, 1992.

Fujita, E. M., Campbell, D. E., Zielinska, B. B., Sagebiel, J. C., Bowen, J. L., Goliff, W. S., Stockwell, W. R. and Lawson, D. R.: Diurnal and weekday variations in the source contributions of ozone precursors in California's South Coast Air Basin, J. Air Waste Manag. Assoc., doi:10.1080/10473289.2003.10466226, 2003.

Fujita, E. M., Stockwell, W. R., Campbell, D. E., Keislar, R. E. and Lawson, D. R.: Evolution of the magnitude and spatial extent of the weekend ozone effect in California's South Coast Air Basin, 1981–2000, J. Air Waste Manag. Assoc., doi:10.1080/10473289.2003.10466225, 2003.

Galbally, I. E. and Roy, C. R.: Loss of fixed nitrogen from soils by nitric oxide exhalation [11], Nature, doi:10.1038/275734a0, 1978.Gallardo, L. and Rodhe, H.: Oxidized nitrogen in the remote Pacific: The role of electrical discharges over the oceans, J. Atmos. Chem., doi:10.1023/A:1005738402496, 1997.

Gallardo, L. and Rodhe, H.: Oxidized nitrogen in the remote Pacific: The role of electrical discharges over the oceans, J. Atmos. Chem., doi:10.1023/A:1005738402496, 1997.

Galloway, J. N. and Cowling, E. B.: Reactive nitrogen and the world: 200 Years of change, in Ambio., 2002.

https://doi.org/10.5194/gmd-2020-415
Preprint. Discussion started: 6 January 2021

Galloway, J. N., Dentener, F. J., Capone, D. G., Boyer, E. W., Howarth, R. W., Seitzinger, S. P., Asner, G. P., Cleveland, C. C., Green, P. A., Holland, E. A., Karl, D. M., Michaels, A. F., Porter, J. H., Townsend, A. R. and Vörösmarty, C. J.: Nitrogen cycles: Past, present, and future, Biogeochemistry, doi:10.1007/s10533-004-0370-0, 2004.

Ganzeveld, L. N., Lelieveld, J., Dentener, F. J., Krol, M. C., Bouwman, A. J. and Roelofs, G. J.: Global soil-biogenic NOX emissions and the role of canopy processes, J. Geophys. Res. Atmos., doi:10.1029/2001JD001289, 2002.

Garten, C. T.: Nitrogen isotope composition of ammonium and nitrate in bulk precipitation and forest throughfall, Int. J. Environ. Anal. Chem., doi:10.1080/03067319208027017, 1992.

Gauss, M., Myhre, G., Isaksen, I. S. A., Grewe, V., Pitari, G., Wild, O., Collins, W. J., Dentener, F. J., Ellingsen, K., Gohar, L. K., Hauglustaine, D. A., Iachetti, D., Lamarque, J. F., Mancini, E., Mickley, L. J., Prather, M. J., Pyle, J. A., Sanderson, M. G., Shine, K. P., Stevenson, D. S., Sudo, K., Szopa, S. and Zeng, G.: Radiative forcing since preindustrial times due to ozone change in the troposphere and the lower stratosphere, Atmos. Chem. Phys., doi:10.5194/acp-6-575-2006, 2006.

Hall, S. J., Ogata, E. M., Weintraub, S. R., Baker, M. A., Ehleringer, J. R., Czimczik, C. I. and Bowling, D. R.: Convergence in nitrogen deposition and cryptic isotopic variation across urban and agricultural valleys in northern Utah, J. Geophys. Res. Biogeosciences, doi:10.1002/2016JG003354, 2016.

Hanson, P. J. and Lindberg, S. E.: Dry deposition of reactive nitrogen compounds: A review of leaf, canopy and non-foliar measurements, Atmos. Environ. Part A, Gen. Top., doi:10.1016/0960-1686(91)90020-8, 1991.

Harley, R. A., McKeen, S. A., Pearson, J., Rodgers, M. O. and Lonneman, W. A.: Analysis of motor vehicle emissions during the Nashville/Middle Tennessee Ozone Study, J. Geophys. Res. Atmos., doi:10.1029/2000JD900677, 2001.

https://doi.org/10.5194/gmd-2020-415
Preprint. Discussion started: 6 January 2021

Heaton, T. H. E.: 15N14N ratios of nitrate and ammonium in rain at Pretoria, South Africa, Atmos. Environ., doi:10.1016/0004-6981(87)90080-1, 1987.

Heaton, T. H. E.: 15N/14N ratios of NOx from vehicle engines and coal-fired power stations, Tellus B, doi:10.1034/j.1600-0889.1990.00007.x-i1, 1990.

Hoering, T.: The isotopic composition of the ammonia and the nitrate ion in rain, Geochim. Cosmochim. Acta, doi:10.1016/0016-7037(57)90021-2, 1957.

Houlton, B. Z., Boyer, E., Finzi, A., Galloway, J., Leach, A., Liptzin, D., Melillo, J., Rosenstock, T. S., Sobota, D. and Townsend, A. R.: Intentional versus unintentional nitrogen use in the United States: Trends, efficiency and implications, Biogeochemistry, doi:10.1007/s10533-012-9801-5, 2013.

Houyoux, M.: Clean Air Interstate Rule Emissions Inventory Technical Support Document. US EPA, 2005.

Hudman, R. C., Moore, N. E., Mebust, A. K., Martin, R. V., Russell, A. R., Valin, L. C. and Cohen, R. C.: Steps towards a mechanistic model of global soil nitric oxide emissions: Implementation and space based-constraints, Atmos. Chem. Phys., doi:10.5194/acp-12-7779-2012, 2012.

Huntrieser, H., Schlager, H., Feigl, C. and Höller, H.: Transport and production of NOX in electrified thunderstorms: Survey of previous studies and new observations at midlatitudes, J. Geophys. Res. Atmos., doi:10.1029/98JD02353, 1998.

Huntrieser, H., Feigl, C., Schlager, H., Schröder, F., Gerbig, C., van Velthoven, P., Flatøy, F., Théry, C., Petzold, A., Höller, H. and Schumann, U.: Airborne measurements of NOx, tracer species, and small particles during the European lightning nitrogen oxides experiment, J. Geophys. Res. Atmos., doi:10.1029/2000jd000209, 2002.

https://doi.org/10.5194/gmd-2020-415
Preprint. Discussion started: 6 January 2021

Ingalls, M. N.: On-road vehicle emission factors from measurements in a Los Angeles area tunnel, in Proceedings - A&WMA Annual Meeting., 1989.

Jacob, D. J. and Wofsy, S. C.: Budgets of reactive nitrogen, hydrocarbons, and ozone over the Amazon forest during the wet season, J. Geophys. Res., doi:10.1029/jd095id10p16737, 1990.

Jaeglé, L., Steinberger, L., Martin, R. V. and Chance, K.: Global partitioning of NOx sources using satellite observations: Relative roles of fossil fuel combustion, biomass burning and soil emissions, in Faraday Discussions., 2005.

Johansson, C.: Pine forest: a negligible sink for atmospheric NO x in rural Sweden , Tellus B Chem. Phys. Meteorol., doi:10.3402/tellusb.v39i5.15360, 1987.

Koike, M., Kondo, Y., Kita, K., Takegawa, N., Nishi, N., Kashihara, T., Kawakami, S., Kudoh, S., Blake, D., Shirai, T., Liley, B., Ko, M. K., Miyazaki, Y., Kawasaki, Z. and Ogawa, T.: Measurements of reactive nitrogen produced by tropical thunderstorms during BIBLE-C, J. Geophys. Res. Atmos., doi:10.1029/2006JD008193, 2007.

Lawrence, M. G., Chameides, W. L., Kasibhatla, P. S., Levy, H. and Moxim, W.: Lightning and atmospheric chemistry: The rate of atmospheric NO production, in Handbook of Atmospheric Electrodynamics., 2017.

Lerdau, M. T., Munger, J. W. and Jacob, D. J.: The NO2 flux conundrum, Science (80-.)., doi:10.1126/science.289.5488.2291, 2000.

Levy, H., Moxim, W. J. and Kasibhatla, P. S.: A global three-dimensional time-dependent lightning source of tropospheric NOx, J. Geophys. Res. Atmos., doi:10.1029/96jd02341, 1996.

Li, D. and Wang, X.: Nitrogen isotopic signature of soil-released nitric oxide (NO) after fertilizer application, Atmos. Environ., doi:10.1016/j.atmosenv.2008.01.042, 2008.

https://doi.org/10.5194/gmd-2020-415
Preprint. Discussion started: 6 January 2021

Li, Y., Schichtel, B. A., Walker, J. T., Schwede, D. B., Chen, X., Lehmann, C. M. B., Puchalski, M. A., Gay, D. A. and Collett, J. L.: Increasing importance of deposition of reduced nitrogen in the United States, Proc. Natl. Acad. Sci. U. S. A., doi:10.1073/pnas.1525736113, 2016.

Liao, T., Gui, K., Jiang, W., Wang, S., Wang, B., Zeng, Z., Che, H., Wang, Y. and Sun, Y.: Air stagnation and its impact on air quality during winter in Sichuan and Chongqing, southwestern China, Sci. Total Environ., doi:10.1016/j.scitotenv.2018.04.122, 2018.

Lighty, J. A. S., Veranth, J. M. and Sarofim, A. F.: Combustion aerosols: Factors governing their size and composition and implications to human health, J. Air Waste Manag. Assoc., doi:10.1080/10473289.2000.10464197, 2000.

Liu, L., Guo, J., Miao, Y., Liu, L., Li, J., Chen, D., He, J. and Cui, C.: Elucidating the relationship between aerosol concentration and summertime boundary layer structure in central China, Environ. Pollut., doi:10.1016/j.envpol.2018.06.008, 2018.

Ludwig, J., Meixner, F. X., Vogel, B. and Forstner, J.: Soil-air exchange of nitric oxide: An overview of processes, environmental factors, and modeling studies, Biogeochemistry, doi:10.1023/A:1006424330555, 2001.

Martin, R. V., Sauvage, B., Folkins, I., Sioris, C. E., Booone, C., Bernath, P. and Ziemke, J.: Space-based constraints on the production of nitric oxide by lightning, J. Geophys. Res. Atmos., doi:10.1029/2006JD007831, 2007.

Mase, D. F.: A coupled modeling and observational approach to understanding oxygen-18 in atmospheric nitrate, Ph. D. thesis, Purdue University, United States of America, 2010.

Miao, Y., Guo, J., Liu, S., Zhao, C., Li, X., Zhang, G., Wei, W. and Ma, Y.: Impacts of synoptic condition and planetary boundary layer structure on the trans-boundary aerosol transport from Beijing-Tianjin-Hebei region to northeast China, Atmos. Environ., doi:10.1016/j.atmosenv.2018.03.005, 2018.

https://doi.org/10.5194/gmd-2020-415
Preprint. Discussion started: 6 January 2021

Miao, Y., Li, J., Miao, S., Che, H., Wang, Y., Zhang, X., Zhu, R. and Liu, S.: Interaction Between Planetary Boundary Layer and PM2.5 Pollution in Megacities in China: a Review, Curr. Pollut. Reports, doi:10.1007/s40726-019-00124-5, 2019.

Michalski, G., Fang, H., Walters, W. W., & Mase, D.: i_N RACM: Incorporating ^{15}N into the Regional Atmospheric Chemistry Mechanism (RACM) for assessing the role photochemistry plays in controlling the isotopic composition of NO_x, NO_y, and atmospheric nitrate, Geoscientific Model Development Discussions, 1-47, 2020.

Miller, D. J., Wojtal, P. K., Clark, S. C. and Hastings, M. G.: Vehicle NOx emission plume isotopic signatures: Spatial variability across the eastern United States, J. Geophys. Res., doi:10.1002/2016JD025877, 2017.

Miller, D. J., Chai, J., Guo, F., Dell, C. J., Karsten, H. and Hastings, M. G.: Isotopic Composition of In Situ Soil NOx Emissions in Manure-Fertilized Cropland, Geophys. Res. Lett., doi:10.1029/2018GL079619, 2018.

Moore, H.: The isotopic composition of ammonia, nitrogen dioxide and nitrate in the atmosphere, Atmos. Environ., doi:10.1016/0004-6981(77)90102-0, 1977.

Muller, J. F.: Geographical distribution and seasonal variation of surface emissions and deposition velocities of atmospheric trace gases, J. Geophys. Res., doi:10.1029/91JD02757, 1992.

Müller, J.-F. and Stavrakou, T.: Inversion of CO and NOx emissions using the adjoint of the IMAGES model, Atmos. Chem. Phys., doi:10.5194/acp-5-1157-2005, 2005.

Murray, L. T.: Lightning NOx and Impacts on Air Quality, Curr. Pollut. Reports, doi:10.1007/s40726-016-0031-7, 2016.

National Centers for Environmental Information: U.S. Wind Climatology, Available from: https://www.ncdc.noaa.gov/societal-impacts/wind/, 2019.

https://doi.org/10.5194/gmd-2020-415
Preprint. Discussion started: 6 January 2021

National Centers for Environmental Information: Model Datasets, available from: https://www.ncdc.noaa.gov/data-access/model-data/model-datasets, 2019.

Occhipinti, C., Aneja, V. P., Showers, W. and Niyogi, D.: Back-trajectory analysis and source-receptor relationships: Particulate matter and nitrogen isotopic composition in rainwater, in Journal of the Air and Waste Management Association., 2008.

Oke, T. R.: Boundary Layer Climates., 2002.

Ott, L. E., Pickering, K. E., Stenchikov, G. L., Huntrieser, H. and Schumann, U.: Effects of lightning NOx production during the 21 July European Lightning Nitrogen Oxides Project storm studied with a three-dimensional cloud-scale chemical transport model, J. Geophys. Res. Atmos., doi:10.1029/2006JD007365, 2007.

Parrish, D. D.: Critical evaluation of US on-road vehicle emission inventories, Atmos. Environ., doi:10.1016/j.atmosenv.2005.11.033, 2006.

Pearson, J., Wells, D. M., Seller, K. J., Bennett, A., Soares, A., Woodall, J. and Ingrouille, M. J.: Traffic exposure increases natural 15N and heavy metal concentrations in mosses, New Phytol., doi:10.1046/j.1469-8137.2000.00702.x, 2000.

Pierce, T. E.: Reconsideration of the Emission Factors assumed in BEIS3 for Three USGS Vegetation Categories: Shrubland, Coniferous Forest, and Deciduous Forest, 2001.

Pierson, W. R., Gertler, A. W. and Bradow, R. L.: Comparison of the scaqs tunnel study with other onroad vehicle emission data, J. Air Waste Manag. Assoc., doi:10.1080/10473289.1990.10466799, 1990.

Pierson, W. R., Gertler, A. W., Robinson, N. F., Sagebiel, J. C., Zielinska, B., Bishop, G. A., Stedman, D. H., Zweidinger, R. B. and Ray, W. D.: Real-world automotive emissions - summary

https://doi.org/10.5194/gmd-2020-415
Preprint. Discussion started: 6 January 2021

of studies in the Fort McHenry and Tuscarora Mountain Tunnels, in Atmospheric Environment., 1996.

Pilegaard, K.: Processes regulating nitric oxide emissions from soils, Philos. Trans. R. Soc. B Biol. Sci., doi:10.1098/rstb.2013.0126, 2013.

Potter, C. S., Matson, P. A., Vitousek, P. M. and Davidson, E. A.: Process modeling of controls on nitrogen trace gas emissions from soils worldwide, J. Geophys. Res. Atmos., doi:10.1029/95JD02028, 1996.

Pouliot, G., & Pierce, T. E.: Integration of the Model of Emissions of Gases and Aerosols from Nature (MEGAN) into the CMAQ Modeling System, in: 18th International Emission Inventory Conference, Baltimore, Maryland, 14 April 2009, 14-17, 2009.

Redling, K., Elliott, E., Bain, D. and Sherwell, J.: Highway contributions to reactive nitrogen deposition: Tracing the fate of vehicular NOx using stable isotopes and plant biomonitors, Biogeochemistry, doi:10.1007/s10533-013-9857-x, 2013.

Riha, K. M.: The use of stable isotopes to constrain the nitrogen cycle, Ph. D. thesis, Purdue University, United States of America, 2013.

Ridley, B. A., Dye, J. E., Walega, J. G., Zheng, J., Grahek, F. E. and Rison, W.: On the production of active nitrogen by thunderstorms over New Mexico, J. Geophys. Res. Atmos., doi:10.1029/96jd01706, 1996.

Ridley, B., Ott, L., Pickering, K., Emmons, L., Montzka, D., Weinheimer, A., Knapp, D., Grahek, F., Li, L., Heymsfield, G., McGill, M., Kucera, P., Mahoney, M. J., Baumgardner, D., Schultz, M. and Brasseur, G.: Florida thunderstorms: A faucet of reactive nitrogen to the upper troposphere, J. Geophys. Res. D Atmos., doi:10.1029/2004JD004769, 2004.

https://doi.org/10.5194/gmd-2020-415
Preprint. Discussion started: 6 January 2021

Russell, K. M., Galloway, J. N., MacKo, S. A., Moody, J. L. and Scudlark, J. R.: Sources of nitrogen in wet deposition to the Chesapeake Bay region, Atmos. Environ., doi:10.1016/S1352-2310(98)00044-2, 1998.

Savard, M. M., Bégin, C., Smirnoff, A., Marion, J. and Rioux-Paquette, E.: Tree-ring nitrogen isotopes reflect anthropogenic NOx emissions and climatic effects, Environ. Sci. Technol., doi:10.1021/es802437k, 2009.

Savard, M. M., Cole, A., Smirnoff, A. and Vet, R.: Δ15N values of atmospheric N species simultaneously collected using sector-based samplers distant from sources – Isotopic inheritance and fractionation, Atmos. Environ., doi:10.1016/j.atmosenv.2017.05.010, 2017.

Sawyer, R. F., Harley, R. A., Cadle, S. H., Norbeck, J. M., Slott, R. and Bravo, H. A.: Mobile sources critical review: 1998 NARSTO assessment, Atmos. Environ., doi:10.1016/S1352-2310(99)00463-X, 2000.

Scholes, M. C., Martin, R., Scholes, R. J., Parsons, D. and Winstead, E.: NO and N2O emissions from savanna soils following the first simulated rains of the season, Nutr. Cycl. Agroecosystems, doi:10.1023/a:1009781420199, 1997.

Schumann, U., Kurz, C., Schlager, H., Huntrieser, H., Emmons, L., Labrador, L., Meijer, E., Ulanovsky, A. and Viciani, S.: Towards a robust estimate of the global lightning nitrogen oxides source rate and its error bound, in European Space Agency, (Special Publication) ESA SP., 2006.

Schumann, U. and Huntrieser, H.: The global lightning-induced nitrogen oxides source, Atmos. Chem. Phys., doi:10.5194/acp-7-3823-2007, 2007.

Schwartz, S. E.: The Whitehouse effect - Shortwave radiative forcing of climate by anthropogenic aerosols: An overview, J. Aerosol Sci., doi:10.1016/0021-8502(95)00533-1, 1996.

Schwede, D., Pouliot, G. and Pierce, T.: Changes to the biogenic emissions inventory system version 3 (BEIS3), in 4th Annual CMAS User's Conference., 2005.

https://doi.org/10.5194/gmd-2020-415
Preprint. Discussion started: 6 January 2021

Shepherd, M. F., Barzetti, S. and Hastie, D. R.: The production of atmospheric NOx and N2O from a fertilized agricultural soil, Atmos. Environ. Part A, Gen. Top., doi:10.1016/0960-1686(91)90277-E, 1991.

Shu, L., Xie, M., Gao, D., Wang, T., Fang, D., Liu, Q., Huang, A. and Peng, L.: Regional severe particle pollution and its association with synoptic weather patterns in the Yangtze River Delta region, China, Atmos. Chem. Phys., doi:10.5194/acp-17-12871-2017, 2017.

Singer, B. C. and Harley, R. A.: A Fuel-Based Motor Vehicle Emission Inventory, J. Air Waste Manag. Assoc., doi:10.1080/10473289.1996.10467492, 1996.

Singer, B. C. and Harley, R. A.: A fuel-based inventory of motor vehicle exhaust emissions in the Los Angeles area during summer 1997, Atmos. Environ., doi:10.1016/S1352-2310(99)00358-1, 2000.

Skamarock, W. C., Dye, J. E., Defer, E., Barth, M. C., Stith, J. L., Ridley, B. A. and Baumann, K.: Observational- and modeling-based budget of lightning-produced NOx in a continental thunderstorm, J. Geophys. Res. Atmos., doi:10.1029/2002jd002163, 2003.

Slovik, S., Siegmund, A., Fuhrer, H. W. and Heber, U.: Stomatal uptake of SO2, NOx and O3 by spruce crowns (Picea abies) and canopy damage in Central Europe, New Phytol., doi:10.1111/j.1469-8137.1996.tb01884.x, 1996.

Snape, C. E., Sun, C., Fallick, A. E., Irons, R. and Haskell, J.: Potential of stable nitrogen isotope ratio measurements to resolve fuel and thermal NOx in coal combustion, Fuel Chem. Div. Prepr., 2003.

Snyder, J. P.: Map projections - a working manual, US Geol. Surv. Prof. Pap., 1987.

Srivastava, R. K., Neuffer, W., Grano, D., Khan, S., Staudt, J. E. and Jozewicz, W.: Controlling NO x emission from industrial sources, Environ. Prog., doi:10.1002/ep.10063, 2005.

https://doi.org/10.5194/gmd-2020-415
Preprint. Discussion started: 6 January 2021

Staudt, A. C., Jacob, D. J., Ravetta, F., Logan, J. A., Bachiochi, D., Sandholm, S., Ridley, B., Singh, H. B. and Talbot, B.: Sources and chemistry of nitrogen oxides over the tropical Pacific, J. Geophys. Res. Atmos., doi:10.1029/2002jd002139, 2003.

Stavrakou, T., Müller, J. F., Boersma, K. F., Van Der A., R. J., Kurokawa, J., Ohara, T. and Zhang, Q.: Key chemical NOx sink uncertainties and how they influence top-down emissions of nitrogen oxides, Atmos. Chem. Phys., doi:10.5194/acp-13-9057-2013, 2013.

Stehfest, E. and Bouwman, L.: N2O and NO emission from agricultural fields and soils under natural vegetation: Summarizing available measurement data and modeling of global annual emissions, Nutr. Cycl. Agroecosystems, doi:10.1007/s10705-006-9000-7, 2006.

Stevenson, D. S., Dentener, F. J., Schultz, M. G., Ellingsen, K., van Noije, T. P. C., Wild, O., Zeng, G., Amann, M., Atherton, C. S., Bell, N., Bergmann, D. J., Bey, I., Butler, T., Cofala, J., Collins, W. J., Derwent, R. G., Doherty, R. M., Drevet, J., Eskes, H. J., Fiore, A. M., Gauss, M., Hauglustaine, D. A., Horowitz, L. W., Isaksen, I. S. A., Krol, M. C., Lamarque, J. F., Lawrence, M. G., Montanaro, V., Müller, J. F., Pitari, G., Prather, M. J., Pyle, J. A., Rast, S., Rodriquez, J. M., Sanderson, M. G., Savage, N. H., Shindell, D. T., Strahan, S. E., Sudo, K. and Szopa, S.: Multimodel ensemble simulations of present-day and near-future tropospheric ozone, J. Geophys. Res. Atmos., doi:10.1029/2005JD006338, 2006.

The Institute for the Environment - The University of North Carolina at Chapel Hill: SMOKE v4.5 User's Manual, Available from: https://www.cmascenter.org/smoke/documentation/4.5/html/, 2017.

Thoene, B., Rennenberg, H. and Weber, P.: Absorption of atmospheric NO2 by spruce (Picea abies) trees: II. Parameterization of NO2 fluxes by controlled dynamic chamber experiments, New Phytol., doi:10.1111/j.1469-8137.1996.tb04630.x, 1996.

Thomas, R. J., Krehbiel, P. R., Rison, W., Hamlin, T., Boccippio, D. J., Goodman, S. J. and Christian, H. J.: Comparison of ground-based 3-dimensional lightning mapping observations

https://doi.org/10.5194/gmd-2020-415
Preprint. Discussion started: 6 January 2021

with satellite-based LIS observations in Oklahoma, Geophys. Res. Lett., doi:10.1029/1999GL010845, 2000.

Tie, X., Zhang, R., Brasseur, G. and Lei, W.: Global NOx production by lightning, J. Atmos. Chem., doi:10.1023/A:1016145719608, 2002.

Tost, H., Jöckel, P. and Lelieveld, J.: Lightning and convection parameterisations - Uncertainties in global modelling, Atmos. Chem. Phys., doi:10.5194/acp-7-4553-2007, 2007.

United States Census Bureau: 2007−2011 American Community Survey 5-Year Estimates, travel time to work by zip code, table B08303, Available from: https://www.census.gov/programs-surveys/acs/technical-documentation/table-and-geography-changes/2011/5-year.html, 2019.

United States Energy Information Administration: Electricity, Available from: https://www.eia.gov/electricity/data/eia860/, 2017a.

United States Energy Information Administration: U.S. electric generating capacity increase in 2016 was largest net change since 2011, Available from: https://www.eia.gov/todayinenergy/detail.php?id=30112, 2017b.

United States Environmental Protection Agency: National Emissions Inventory (NEI), Available from: https://www.epa.gov/air-emissions-inventories/national-emissions-inventory-nei, 2014.

United States Environmental Protection Agency: Biogenic Emissions Landuse Database, Available from: https://www.epa.gov/air-emissions-modeling/biogenic-emissions-landuse-database-version-3-beld3, 2018.

US Environmental Protection Agency: User's Guide to MOBILE6.1 and MOBILE6.2 Mobile Source Emission Factor Model, Tech. Rep. EPA420-R-03-010, 2003.

Van Noije, T. P. C., Eskes, H. J., Dentener, F. J., Stevenson, D. S., Ellingsen, K., Schultz, M. G., Wild, O., Amann, M., Atherton, C. S., Bergmann, D. J., Bey, I., Boersma, K. F., Butler, T.,

https://doi.org/10.5194/gmd-2020-415
Preprint. Discussion started: 6 January 2021

Cofala, J., Drevet, J., Fiore, A. M., Gauss, M., Hauglustaine, D. A., Horowitz, L. W., Isaksen, I. S. A., Krol, M. C., Lamarque, J. F., Lawrence, M. G., Martin, R. V., Montanaro, V., Müller, J. F., Pitari, G., Prather, M. J., Pyle, J. A., Richter, A., Rodriguez, J. M., Savage, N. H., Strahan, S. E., Sudo, K., Szopa, S. and Van Roozendael, M.: Multi-model ensemble simulations of tropospheric NO2 compared with GOME retrievals for the year 2000, Atmos. Chem. Phys., doi:10.5194/acp-6-2943-2006, 2006.

Vukovich, J., & Pierce, T.: The implementation of BEIS3 within the SMOKE modeling framework, in: Proceedings of the 11th International Emissions Inventory Conference, Atlanta, Georgia, 15 April 2002, 15-18, 2002.

Walters, W. W., Goodwin, S. R. and Michalski, G.: Nitrogen stable isotope composition (δ15N) of vehicle-emitted NOx, Environ. Sci. Technol., doi:10.1021/es505580v, 2015a.

Walters, W. W., Tharp, B. D., Fang, H., Kozak, B. J. and Michalski, G.: Nitrogen Isotope Composition of Thermally Produced NOx from Various Fossil-Fuel Combustion Sources, Environ. Sci. Technol., doi:10.1021/acs.est.5b02769, 2015b.

Walters, W. W., Fang, H. and Michalski, G.: Summertime diurnal variations in the isotopic composition of atmospheric nitrogen dioxide at a small midwestern United States city, Atmos. Environ., doi:10.1016/j.atmosenv.2018.01.047, 2018.

Weber, P. and Rennenberg, H.: Dependency of nitrogen dioxide (NO2) fluxes to wheat (Triticum aestivum L.) leaves from NO2 concentration, light intensity, temperature and relative humidity determined from controlled dynamic chamber experiments, Atmos. Environ., doi:10.1016/1352-2310(96)00008-8, 1996.

Wong, S., Wang, W. C., Isaksen, I. S. A., Berntsen, T. K. and Sundet, J. K.: A global climate-chemistry model study of present-day tropospheric chemistry and radiative forcing from changes in tropospheric O3 since the preindustrial period, J. Geophys. Res. D Atmos., doi:10.1029/2003JD003998, 2004.

https://doi.org/10.5194/gmd-2020-415
Preprint. Discussion started: 6 January 2021

Xing, J., Pleim, J., Mathur, R., Pouliot, G., Hogrefe, C., Gan, C. M. and Wei, C.: Historical gaseous and primary aerosol emissions in the United States from 1990 to 2010, Atmos. Chem. Phys., doi:10.5194/acp-13-7531-2013, 2013.

Yan, X., Ohara, T. and Akimoto, H.: Statistical modeling of global soil NOX emissions, Global Biogeochem. Cycles, doi:10.1029/2004GB002276, 2005.

Yienger, J. J. and Levy, H.: Empirical model of global soil-biogenic NOx emissions, J. Geophys. Res., doi:10.1029/95jd00370, 1995.

Yu, Z. and Elliott, E. M.: Novel Method for Nitrogen Isotopic Analysis of Soil-Emitted Nitric Oxide, Environ. Sci. Technol., doi:10.1021/acs.est.7b00592, 2017.

Zörner, J., Penning de Vries, M. J. M., Beirle, S., Sihler, H., Veres, P. R., Williams, J. and Wagner, T.: Multi-satellite sensor study on precipitation-induced emission pulses of NO_x from soils in semi-arid ecosystems, Atmos. Chem. Phys. Discuss., doi:10.5194/acp-2016-93, 2016.